Adaptive pitch control for ships with diesel mechanical and hybrid propulsion

Geertsma, R. D.; Visser, K.; Negenborn, R. R.

DOI
10.1016/j.apenergy.2018.07.080

Publication date
2018

Document Version
Final published version

Published in
Applied Energy

Applied Energy 228 (2018) 2490–2509

Contents lists available at ScienceDirect

Applied Energy

journal homepage: www.elsevier.com/locate/apenergy

Adaptive pitch control for ships with diesel mechanical and hybrid propulsion

R.D. Geertsma[a,b,*], K. Visser[a,b], R.R. Negenborn[a]

[a] Department of Maritime & Transport Technology, Delft University of Technology, The Netherlands
[b] Faculty of Military Sciences, Netherlands Defence Academy, The Netherlands

HIGHLIGHTS

- A novel adaptive pitch control strategy is proposed.
- Fuel consumption, CO_2, NO_x and PM emissions are reduced.
- Improved acceleration and consistently limited thermal loading is demonstrated.
- The approach can save 5–15% fuel and emissions and reduce acceleration time by 30%.
- No more operator input is required to switch between fast and efficient sailing.

ARTICLE INFO

Keywords:
Mechanical propulsion
Non-linear control systems
Marine systems
Modelling and simulation
Emission reduction
Autonomous systems

ABSTRACT

Shipping urgently needs to reduce its impact on the environment, both due to CO_2, NO_x and particulate matter (PM) emissions and due to underwater noise. On the other hand, multifunction ships such as offshore support vessels, anchor handling and towing vessels, naval vessels and wind farm construction and support vessels require fast and accurate manoeuvring and need highly reliable systems to support reduced or no crew. Diesel mechanical propulsion with controllable pitch propellers provides high efficiency and low CO_2 emissions, but has traditionally been poor in manoeuvrability, can suffer from thermal overloading due to manoeuvring and requires significant measures to meet NO_x and PM emission regulations. The control strategy of diesel mechanical propulsion with fixed combinator curves is one of the causes of the poor manoeuvrability, thermal overloading and cavitation noise during manoeuvring, such as slam start and intermediate acceleration manoeuvres. This paper proposes an adaptive pitch control strategy with slow integrating speed control that reduces fuel consumption, CO_2, NO_x and PM emissions and underwater noise, improves acceleration performance, limits engine loading and prevents engine under- and overspeed. A simulation study with a validated model of a case study *Holland class* Patrol Vessel demonstrates 5–15% reduction in fuel consumption and CO_2 emissions, compared to the baseline transit control mode in the ship speed range from 6 to 15 kts, during constant speed sailing. Moreover, the adaptive pitch control strategy reduces acceleration time from 0 to 15 kts with the slam start procedure by 32% compared to the baseline manoeuvre control mode and by 84% for an intermediate acceleration from 10 to 15 kts, while preventing thermal overloading of the engine, during straight line manoeuvres. Combining this control strategy with hybrid propulsion, running an electric drive in parallel with the propulsion diesel engine, can potentially further reduce fuel consumption at low speeds while also improving acceleration performance even more. Therefore, hybrid propulsion plants with controllable pitch propellers and adaptive pitch control can provide a significant contribution to the urgent reduction of environmental impact of shipping and to the need for more autonomous and reliable ship systems.

1. Introduction

The United Nations emissions gap report [1] identifies an urgent need to increase the reduction in CO_2 emissions across the globe to meet the goals of the Paris Agreement. Thus, the 72nd Marine Environmental Protection Committee meeting of the International Maritime Organisation (IMO) agreed to 'reduce total annual global shipping emissions by 50% over 2008 by 2050', in its *initial strategy on greenhouse*

* Corresponding author at: Delft University of Technology, Faculty of 3ME, Building 34, Mekelweg 2, 2628CD Delft, The Netherlands.
E-mail address: r.d.geertsma@tudelft.nl (R.D. Geertsma).

https://doi.org/10.1016/j.apenergy.2018.07.080
Received 19 April 2018; Received in revised form 26 June 2018; Accepted 14 July 2018

Nomenclature

Greek Symbols

α_{eff}	effective angle of attack in deg
α_i	shock free entry angle onto the leading edge of the propeller profile in deg
α_{wk}	angle of the vertical wave movement at the propeller centre in rad
β	hydrodynamic pitch angle in rad
λ	air excess ratio
ω_{wv}	wave radial frequency in rad/s
ρ_{sw}	density of seawater in kg/m^3
σ_f	stoichiometric air fuel ratio of the fuel
σ_n	cavitation number
θ	pitch angle in rad
θ_{red}	pitch angle reduction in rad
ζ	significant wave amplitude in m

Roman Symbols

c_1	Vrijdag coefficient to calibrate the effective angle of attack
D_p	propeller diameter in m
f_w	wake fraction
g	standard gravity in m/s^2
i_{gb}	gearbox reduction ratio
K_I	reset rate
K_Q	propeller torque coefficient
k_w	wave number in 1/m
m_1	trapped mass at the start of compression in kg
M_e	engine torque in Nm
m_f	fuel injection per cylinder per cycle in kg
M_p	propeller torque in Nm
n_e	engine speed in Hz
n_p	shaft speed in Hz
n_{virt}	virtual shaft speed in Hz
p_1	charge air pressure in Pa
p_6	average pressure in the cylinder during exhaust opening in Pa
p_∞	ambient water pressure at the center-line of the propeller in Pa
p_v	vapour pressure of water at ambient temperature in Pa
p_d	pressure in the exhaust receiver in Pa
P_{os}	overspeed limitation gain
$P_{pd,0}$	pitch ratio at which zero thrust is achieved
P_{pd}	propeller pitch ratio
P_{us}	under-speed limitation gain
Q_p	open water propeller torque in kNm
q_{23}	specific heat release at constant volume in kJ/kg
q_{34}	specific heat release at constant pressure in kJ/kg
q_{45}	specific heat release at constant temperature in kJ/kg
R_a	gas constant of air in J/kgK
R_v	ship resistance in N
$R_{X,cav}$	fuel increase rate limitation to prevent cavitation
$R_{X,therm}$	fuel increase rate limitation to prevent thermal overloading
T_1	temperature at the start of compression in K
T_6	average temperature in the cylinder during exhaust opening in K
T_p	propeller thrust in N
V_1	cylinder volume at the start of compression in m^3
v_a	advance speed of water into the propeller in m/s
v_s	ship speed in m/s
v_w	wakefield disturbance due to waves in m/s
w_i	specific indicated work during the Seiliger cycle in kNm/kg
X_I	fuel injection setpoint from integrating speed control in %
X_{PI}	fuel injection setpoint from fast *PI* speed control in %
$X_{lim,\lambda}$	fuel injection limitation to limit air excess ratio λ in % of nominal
X_{set}	fuel injection setpoint in % of nominal fuel injection
z	water depth in m at propeller center

Superscripts

*	normalised relative to nominal value

Subscripts

ic	slow integrating speed control
max	maximum
mins	minimum speed setpoint
min	minimum
os	overspeed
set	setpoint
max	maximum value
nom	nominal value

gas emissions reduction for ships [2]. While improved planning of vessel operations [3,4], either with manned or autonomous vessels [5,6], and improved route planning [7], taking into account weather and loading conditions [8–10] can all help reduce emissions, single ships also need to reduce their emissions for a given operating profile with advances in power and propulsion systems [11]. Economic studies suggest that, in shipping, the transition to alternative fuels, such as LNG, bio-methanol or synthetic fuels, will be gradual and that diesel engines will continue to provide most propulsion and electric power over the next decades [12]. Therefore, increasing efficiency of diesel mechanical and hybrid propulsion is even more important.

According to estimates in the UN emission gap report, shipping can contribute 0.7 $GtCO_2$ emission reduction by increasing its efficiency [1]. Brynolf et al. [13] provide estimates of the energy efficiency improvement potential of various design and operation aspects. While the savings potential of most design aspects, such as waste heat recovery [14–18], hull coatings and lubrications, hybrid power supply [19–21] and hull design have been quantified in [13,22], the savings potential of engine-propeller interaction is qualified as significant, but not yet quantified [23]. Geertsma et al. [24] quantify a savings potential for pitch control of up to 30% at certain speeds and operating modes for vessels with diesel mechanical propulsion and high manoeuvrability requirements, at the expense of slow acceleration and increased engine thermal loading. How these fuel savings can be achieved while also accelerating fast and limiting engine thermal loading has so far not been addressed.

1.1. Literature review

The most applied control strategy for pitch control is the use of a fixed relationship between the setpoint: lever position or virtual shaft speed; and the control actions: propeller pitch ratio and engine speed [25–27,21]. The optimum propeller pitch ratio and gearbox ratio is then determined for the design point of the propulsion plant, according to the matching procedure proposed in [28] or, alternatively, in [29].Vrijdag et al. [30] conclude that one combinator curve cannot achieve optimal cavitation performance while maintaining engine loading limitations across all operating conditions, due to variations in

weather, ship loading and hull fouling. Therefore, Vrijdag et al. [31] propose a control strategy that maintains an optimum inflow angle of the water onto the propeller blade, *angle of attack*, in the pitch control region of the combinator, and demonstrates the feasibility of this approach in sea trials. The sea trials, in combination with simulation studies, also demonstrate that the engines are not thermally overloaded and acceleration performance improves significantly [32–34]. The impact on fuel consumption of the ship and the influence of the primary engine speed control strategy on system dynamics were not addressed.

While engine speed control is used as a standard for propulsion engines due to its robust control and under- and overspeed protection [21], speed control does lead to significant and potentially damaging load disturbances in waves [35–39]. Alternative speed control strategies, such as H_∞ state feedback control [40], optimal speed feedback using speed signal amplification [39], multivariable adaptive extremum engine control [41] and Multiple Input and Multiple Output (MIMO) optimal speed and pitch H_∞ control [38], can all reduce the load fluctuation, but still aim to reject disturbance of engine speed due to waves with fuel injection control action. While a multivariable control scheme utilising a variable geometry turbocharger can improve manoeuvrability while maintaining smoke emission constraints, as proposed in [42], this requires a diesel engine with variable geometry turbocharger. Similarly, adaptive feedforward control of exhaust gas recirculation can reduce emissions in large diesel engines, but only if equipped with exhaust gas recirculation [43].

Alternatively, Sorensen and Smogelli [44] found that, for electric propulsion, primary control based on torque, power or combined torque-and-power control all gave less thrust, torque and power variance in waves than speed control, while accurately following thrust commands. While a slight increase in shaft speed fluctuation was observed, the stable nature of the propulsion system ensured shaft speed oscillations remained acceptable. For extreme situations, such as propeller emergence, thrust loss estimation and anti-spin thruster control can be added to prevent overspeed and thrust loss [45–47]. Similarly, Coraddu et al. [23] demonstrated with both simulation model experiments and free running model tests that torque and power control leads to lower load fluctuation in turns. Moreover, Blanke et al. [48] demonstrated in a tow-tank test environment that the propeller efficiency in moderate waves increases with up to 2% for torque control compared to speed control, due to the variation in advance speed from waves. Similarly, torque or power control for propulsion diesel engines has been reported by [35,49,50]. Both Faber [35] and Blanke and Nielsen [49] discuss how power control can lead to reduced loading and thermal fluctuations on propulsion diesel engines, but neither quantify the variance reduction or demonstrate the feasibility. Geertsma et al. [50] propose torque control and demonstrate torque control can eliminate thermal loading fluctuation due to waves and significantly reduce cylinder peak temperatures. However, practical feasibility and implementation with pitch control were not addressed.

1.2. Aim and contribution

While shipping urgently has to reduce its environmental impact due to emissions and underwater noise, many ship types, such as offshore vessels, interterminal transport vessels, windturbine construction and support vessels, ferries, and naval vessels also require fast and accurate manoeuvring and reduced maintenance to support reduced maintenance and autonomous shipping [5,51]. This study investigates how much fuel consumption and emissions can be reduced with the novel *adaptive pitch control* strategy, while also improving straight line manoeuvring performance and limiting engine thermal loading. Moreover, settings for this control strategy are proposed that minimise risk of propeller cavitation.

The novelty of this work is threefold: First, we propose a novel adaptive pitch control strategy for diesel mechanical and hybrid propulsion with controllable pitch propellers, which combines the angle of attack approach for propeller pitch control [31] with slow integrating speed control for diesel engine fuel injection. Secondly, we demonstrate how this approach can be used in a control strategy that works across the speed range of the ship to reduce fuel consumption and CO_2 emissions and increase acceleration performance, while consistently limiting engine thermal loading. Finally, we quantify performance improvement with the proposed control strategy for a case study patrol vessel compared to the current baseline control strategy.

1.3. Outline

The paper is organised as follows: in Section 2, we describe the diesel mechanical propulsion system with controllable pitch propeller of the case study Patrol Vessel, its modelling and model validation; in Section 3, we introduce the proposed control strategy and establish its settings; in Section 4, we evaluate the control strategy and compare its performance with the baseline control strategy of the case study Patrol Vessel; and finally, in Section 5, we present the main conclusions and discuss recommendations for further work.

2. System description

Diesel mechanical or hybrid propulsion with controllable pitch propellers typically consists of two shafts with controllable pitch propellers, a gearbox, and one or multiple diesel engines per shaft, as illustrated in Fig. 1. The two shafts with controllable pitch propellers provide redundancy and manoeuvrability. The gearbox is required to reduce engine speed to the lower propeller speed, as we do not consider large transport ships with slow speed two stroke engines. This configuration is typical for the multifunction ships that require silent, manoeuvrable, highly reliable and low emission propulsion.

2.1. Propulsion system model

Propulsion system performance is investigated using the modular, hierarchical and causal propulsion system model proposed and validated in [24]. The diesel mechanical propulsion system model is illustrated schematically in Fig. 3. In the modular, hierarchical and causal modelling paradigm proposed in [52], the direction of the arrows illustrates the causality of the coupled effort and flow variables. The torque M_e from the diesel engine model drives gearbox and shaftline dynamics, resulting in engine speed n_e in Hz. Subsequently, shaft speed n_p determines propeller torque M_p of the propeller model, and propeller thrust T_p drives ship speed v_s in m/s through the hull dynamics. Waves act as a disturbance on the propeller with wave orbital speed v_w and added resistance in the resistance function $R_v(v_s)$. The fuel injection setpoint X_{set} in % and pitch ratio setpoint $P_{p,set}$ act as control actions on the system, while the operator provides the control reference virtual shaft speed n_{virt} in rps. This virtual shaft speed is the fictive shaft speed that results from the product of propeller pitch ratio P_p and shaft speed n_p, as follows:

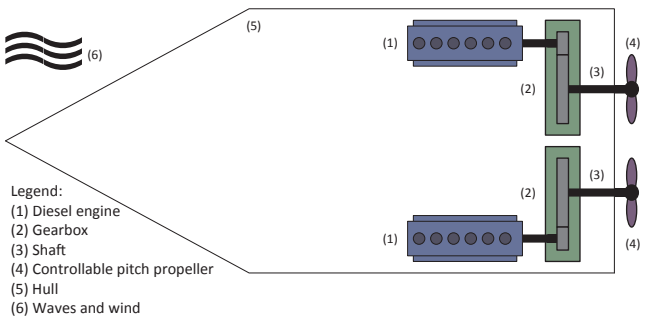

Fig. 1. Typical mechanical propulsion system layout for a ship, from [50].

Fig. 2. HNLMS Holland.

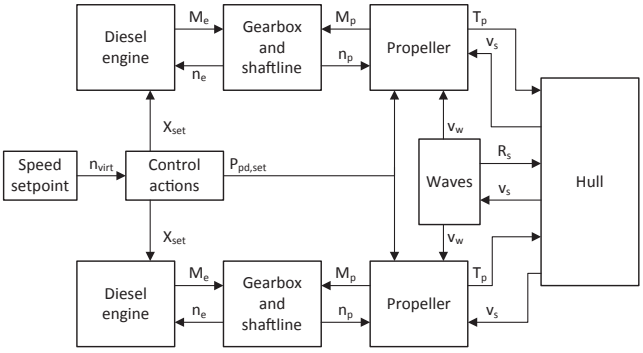

Fig. 3. Schematic presentation of direct drive propulsion system for naval vessel showing causal coupling between models.

$$n_{\mathrm{virt}}(t) = \frac{P_{\mathrm{pd}}(t) - P_{\mathrm{pd},0}}{P_{\mathrm{pd,nom}}} - P_{\mathrm{pd},0} n_{\mathrm{p}(t)}, \tag{1}$$

where P_{pd_0} is the pitch ratio at which zero thrust is achieved and $P_{\mathrm{pd,nom}}$ is the nominal pitch ratio.

For the complete description of the model we refer to [24]. The wave model was improved to include the state wakefield disturbance due to waves v_w in m/s and better represent the dynamic behaviour of waves as a function of ship speed v_s in m/s and wave radial frequency ω_{wv} in rad/s. In this section, we will summarise the model and its sub-models and discuss the wave model improvement to this model.

2.1.1. Diesel engine

The diesel engine model is a mean value first principle model with state variables fuel injection per cylinder per cycle m_{f} in kg, charge air pressure p_1 in Pa and pressure in the exhaust receiver p_d in Pa. The model assumes an ideal gas, perfect scavenging, the six point Seiliger cycle, Büchi power and flow balance between compressor and turbine, Zinner blowdown for the temperature in the exhaust receiver and isentropic expansion with heat loss in the turbocharger. The model thus consists of a system of differential and algebraic equations with three state variables, control action fuel injection setpoint X_{set} in %, input engine speed n_{e} in Hz and output engine torque M_{e} in kNm, and is described in detail in [24].

This mean value first principle model accurately represents mean values of engine efficiencies, temperatures, cylinder and scavenging flows and turbocharger pressures, based on calibration with FAT results. The model does not accurately capture all physical mechanisms, such as the turbocharger equation of motion and the gas exchange mechanism [53], as the models using compressor and turbine maps in [54–56]. This results in a significant reduction in simulation time to generate the performance map, shown in Fig. 9, from hours with the model in [56] to 23 s with this model. This reduced simulation time allows investigating hull-propeller-engine interaction shown in Fig. 4, and the benchmark manoeuvres proposed in [24]. Moreover, the model does not capture crank angle dynamics as in [57,58], combustion dynamics as in [59,60], or fluid dynamics as in [61]. For a short review of diesel engine models, we refer to [24].

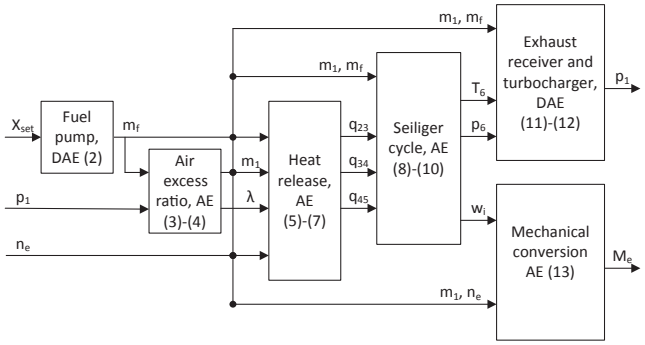

Fig. 4. Schematic presentation of the diesel engine model and the interaction between its subsystems, consisting of Algebraic Equations (AE) or Differential and Algebraic Equations (DAE).

The schematic presentation in Fig. 4 provides the interaction between the engine model subsystems and the governing equations as described in [24]. The summarising equations are as follows:

$$\frac{dm_{\mathrm{f}}(t)}{dt} = f_1(X_{\mathrm{set}}(t),\, m_{\mathrm{f}}(t)) \tag{2}$$

$$m_1(t) = f_2(m_{\mathrm{f}}(t),\, p_1(t),\, n_{\mathrm{e}}(t)) \tag{3}$$

$$\lambda(t) = f_3(m_{\mathrm{f}}(t),\, p_1(t),\, n_{\mathrm{e}}(t)) \tag{4}$$

$$q_{23}(t) = f_4(m_{\mathrm{f}}(t),\, m_1(t),\, n_{\mathrm{e}}(t)) \tag{5}$$

$$q_{34}(t) = f_5(m_{\mathrm{f}}(t),\, m_1(t),\, n_{\mathrm{e}}(t)) \tag{6}$$

$$q_{45}(t) = f_6(m_{\mathrm{f}}(t),\, m_1(t),\, n_{\mathrm{e}}(t)) \tag{7}$$

$$T_6(t) = f_7(m_{\mathrm{f}}(t),\, m_1(t),\, q_{23}(t),\, q_{34}(t),\, q_{45}(t)) \tag{8}$$

$$p_6(t) = f_8(m_{\mathrm{f}}(t),\, m_1(t),\, q_{23}(t),\, q_{34}(t),\, q_{45}(t)) \tag{9}$$

$$w_{\mathrm{i}}(t) = f_9(m_{\mathrm{f}}(t),\, m_1(t),\, q_{23}(t),\, q_{34}(t),\, q_{45}(t)) \tag{10}$$

$$\frac{dp_d(t)}{dt} = f_{10}(m_{\mathrm{f}}(t),\, m_1(t),\, T_6(t),\, p_6(t)) \tag{11}$$

$$\frac{dp_1(t)}{dt} = f_{11}(m_{\mathrm{f}}(t),\, m_1(t),\, T_6(t),\, p_d(t)) \tag{12}$$

$$M_{\mathrm{e}}(t) = f_{12}(w_{\mathrm{i}}(t),\, m_1(t),\, n_{\mathrm{e}}(t)), \tag{13}$$

where m_1 is the trapped mass at the start of compression in kg, λ is the air excess ratio, q_{23} is the specific heat release at constant volume in kJ/kg, from state 2 to state 3 of the Seiliger cycle, q_{34} is the specific heat release at constant pressure in kJ/kg, from state 3 to state 4 of the Seiliger cycle, q_{45} is the specific heat release at constant temperature in kJ/kg, from state 4 to state 5 of the Seiliger cycle, T_6 and p_6 are the average temperature and pressure in the cylinder during exhaust opening in K and Pa, at state 6 of the Seiliger cycle, and w_{i} is the specific indicated work during the complete Seiliger cycle in kNm/kg.

2.1.2. Gearbox and shaft-line

The gearbox and shaft-line model consists of the equation of motion for shaft-line dynamics, assuming rigid coupling between the engine, gearbox, shaft-line and propeller, a linear torque loss model based on [62] and constant relative shaft-line losses. This model thus consists of a system of differential and algebraic equations with as inputs engine and propeller torque M_{e} and M_{p} in kNm, as state variable shaft speed n_{p} in

Hz and as outputs shaft propeller speed and engine speed n_p and n_e in Hz [24]. The summarising equation is as follows:

$$\frac{dn_p(t)}{dt} = f_{13}(M_e(t), M_p(t)). \tag{14}$$

2.1.3. Propeller

The propeller model uses the well-established open water test results and in particular the Wageningen C-series for Controllable Pitch Propellers [63,64]. For the pitch actuation system the model assumes a linear first order transfer function with a fixed time constant τ_P to represent the time delay between changing the pitch setpoint and the actual movement of the pitch [24,65–67,27]. Thus, the propeller model consists of a system of differential and algebraic equations with state variable propeller pitch ratio P_{pd}, control action propeller pitch ratio setpoint $P_{pd,set}$, input variables propeller speed n_p in Hz, ship speed v_s in m/s and wave orbital speed v_w in m/s, and output variables propeller torque M_p in kNm and propeller thrust T_p in kN, represented by the following summarising equations:

$$\frac{dP_{pd}(t)}{dt} = f_{14}(P_{pd}(t), P_{pd_{set}}(t)) \tag{15}$$

$$M_p = f_{15}(P_{pd}(t), n_p(t), v_s(t), v_w(t)) \tag{16}$$

$$T_p = f_{16}(P_{pd}(t), n_p(t), v_s(t), v_w(t)). \tag{17}$$

2.1.4. Hull

The hull model represents ship motion in surge direction, as surge is most relevant for engine loading and loading effects due to turning can be represented as a disturbance after establishing its magnitude with 6 degrees of freedom models [68,27] or by applying a wake fraction variation δw, as proposed in [23]. The size of these wake variations can then be estimated based on the general trends reported in [23], although in this work we only consider straight line acceleration. The model represents the equation of motion with a system of differential and algebraic equations, including state variable ship speed v_s, input variables ship resistance $R(v_s)$ in kN and propeller thrust T_p in kN, and output variable ship speed v_s in m/s. The summarising equation is as follows [24]:

$$\frac{dv_s(t)}{dt} = f_{17}(R(v_s(t)), T_p(t)). \tag{18}$$

2.1.5. Waves

The wave model takes two disturbances into account: the added resistance due to sea state, wind speed, fouling and displacement and the disturbance on the average speed of the water entering the propeller [24]. Additional effects, such as variances in the mean wake speed as a result of the pitching motion of the ship [69] or oblique inflow into the propeller [70] are neglected. The main cause of the disturbance on engine loading is the fluctuating wake speed of the water flowing into the propeller, as previously discussed in [50]. The orbital movement of water causes a disturbance on the average speed of the water entering the propeller, an exponential distribution of water speed along the depth of the propeller and an oblique inflow. In this study, we are interested in the significant disturbance of the wave orbital movement on the propeller loading, due to the significant wave height. We therefore consider the wake speed relative to the propeller center v_w in m/s, as follows [71,72]:

$$v_w(t) = \zeta\omega_{wv} e^{k_w z}\cos(\alpha_{wk}(t)) \tag{19}$$

$$\frac{d\alpha_{wk}(t)}{dt} = k_w v_s(t) + \omega_{wv} \tag{20}$$

$$k_w = \frac{\omega_{wv}^2}{g}, \tag{21}$$

where ζ is the significant wave amplitude in m, ω_{wv} is the wave radial frequency in rad/s, k_w is the wave number in 1/m, z is the water depth in m at the propeller center, α_{wk} is the angle of the vertical wave movement at the propeller centre in rad, and g is the standard gravity in m/s^2.

The resulting model consists of a system of differential and algebraic equations with state variable angle of the vertical wave movement α_{wk}, input ship speed v_s in m/s, and output wake speed disturbance due to waves v_{wk} in m/s. The summarising equations are as follows:

$$\frac{d\alpha_{wk}(t)}{dt} = f_{18}(\alpha_{wk}(t), v_s(t)) \tag{22}$$

$$v_{wk} = f_{19}(t)(\alpha_{wk}(t)). \tag{23}$$

2.2. Baseline conventional control

The baseline conventional control strategy using two fixed combinator curves, rate limitations for acceleration and deceleration, and a pitch reduction strategy to prevent thermal overloading of the engine is described in [24]. The schematic representation of this control strategy is illustrated in Fig. 5 and the combinator curves for the case study patrol vessel are illustrated in Fig. 6. The transit mode aims to provide 'high propulsion efficiency within engine overloading limitations in design conditions' and the manoeuvring mode aims to provide 'high manoeuvrability within engine overloading limitations in design conditions' [24].

The control objectives and the tuning of the baseline conventional control strategy have been described in [73] and the resulting parameters are described and listed in [24]. In summary, the tuning procedure has led to conservative settings, in order to prevent overloading in the worst possible operating conditions. While the risk of thermal overloading has been eliminated, this might lead to reduced performance on Measures of Effectiveness [74] manoeuvrability, cavitation noise and fuel consumption. Ref. [24] concluded that the two operating modes led to very significant differences in performance: the transit mode reduces fuel consumption by up to 30% at 7 kts ship speed, reduces engine thermal loading by 90 K and reduces the risk of cavitation,

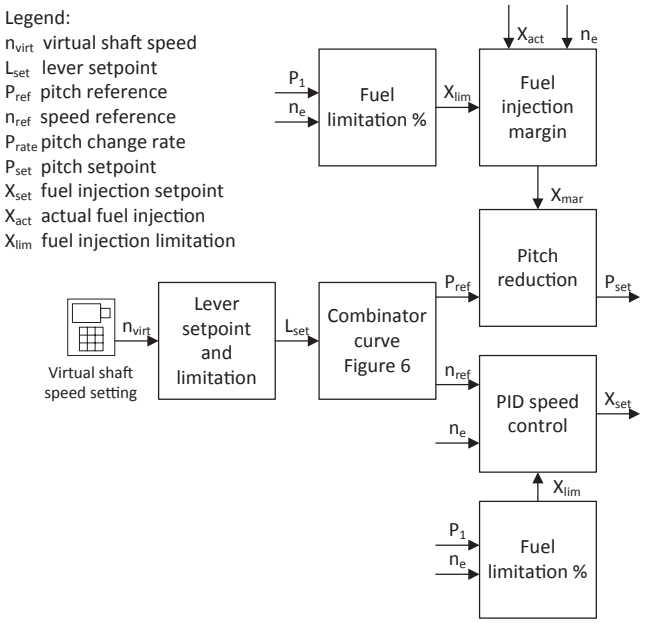

Fig. 5. Schematic representation of baseline control strategy for diesel mechanical propulsion with CPP.

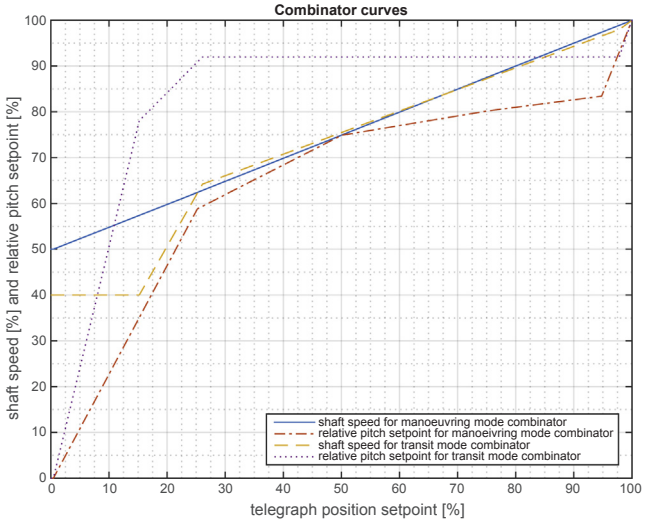

Fig. 6. Combinator curves for baseline control strategy in manoeuvring and transit modes.

while the manoeuvring mode reduces acceleration time from 0 to 15 kts by 41% compared to the transit mode.

2.3. Model validation

This model was validated with a case study Patrol Vessel, shown in Fig. 2, as described extensively in [24]. The diesel engine model (2)–(13) has been validated with Factory Acceptance Test measurements of the main diesel engines and the integrated propulsion system model consisting of (2)–(13), (14), (15)–(17), ()(18)–(21), with Sea Acceptance Trial measurements of the case study *Holland-class* Patrol Vessel, shown in Fig. 2. The model validation used the baseline conventional control strategy of the actual vessel described in Section 2.2. The parameters used for the model and the baseline control strategy are also described in detail in [24]. The validation demonstrates that 'the propulsion system model credibly predicts propulsion system behaviour within 5% accuracy' [24]. Moreover, the comparison of the model performance in waves with measurements on a *Doorman* class frigate as reported in [24], demonstrates the size and orientation of the ellipses in waves of sea state 6, which can also be observed for sea state 4 in Fig. 22, is representative for the effect in real waves, although quantification is not possible, as the exact wave height was not measured during the measurements at sea.

3. Adaptive pitch control strategy

The adaptive pitch control strategy aims to achieve many control objectives with essentially the same control actions as the baseline pitch control strategy. These control actions are propeller pitch ratio setpoint and fuel pump injection setpoint: $u(t) = [P_{p,set}, X_{set}]$. While the baseline control strategy uses measured system outputs propeller pitch ratio P_p and engine speed n_e, the adaptive pitch control strategy additionally uses the estimated hydrodynamic pitch angle: $z(t) = [P_p, n_e, \beta]$. The comparison of the simplified representation of both feedback control strategies is presented in Fig. 7. The following section extensively discusses the control objectives and how the proposed adaptive pitch control strategy achieves highly improved and near optimal performance for these objectives, within the physical limitations of the propulsion system components.

3.1. Control objectives

The control objective for the adaptive pitch control strategy is to optimise for the Measures of Effectiveness (MOEs) fuel consumption, manoeuvrability, engine thermal loading and, in some cases, cavitation noise, while providing the requested virtual shaft speed. In order to quantify the performance against these MOEs, we use the Measures of Performance (MOPs) [74] proposed in [24]. The control objectives derived from these MOPs are:

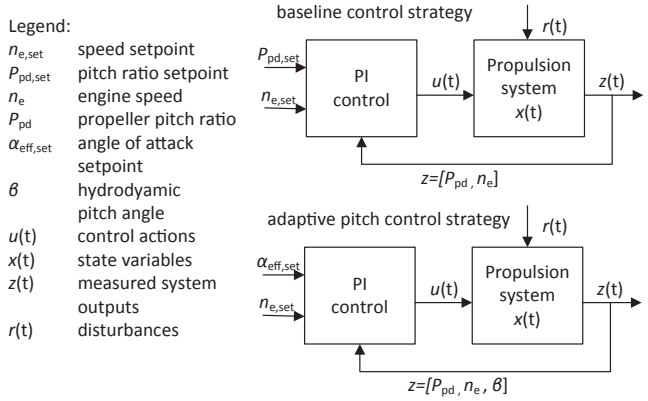

Fig. 7. Simplified representation of baseline control strategy and proposed adaptive pitch control strategy for diesel mechanical propulsion with CPP.

1. Provide requested virtual shaft speed n_{virt} as defined in (1) [31].
2. Maintain operation within the cavitation bucket for the widest possible operating conditions.
3. Minimise fuel consumption across the ship speed profile and for all operating conditions.
4. Maintain engine air excess ratio λ within predefined limits. We will investigate system performance against a number of minimum values of the air excess ratio λ.
5. Prevent engine overspeed and under-speed.

The proposed control strategy is presented schematically in Fig. 8. Next, we will discuss the proposed control laws and constraints, and how they achieve the control objectives.

3.1.1. Virtual shaft speed

The first control objective is to provide the requested virtual shaft speed as defined in (1). In the conventional control strategy, this is achieved with fixed combinator curves, as shown in Fig. 6. While the proposed adaptive pitch control strategy changes pitch based on operating conditions, the speed setpoint needs to be adjusted to compensate pitch changes. Therefore, the speed setpoint is determined from the actual pitch, as previously proposed in [31], as follows:

$$n_{set}(t) = \frac{P_{pd,nom} - P_{pd,0}}{P_{pd}(t) - P_{pd,0}} n_{virt,set}(t). \tag{24}$$

3.1.2. Maintain operation within the cavitation bucket

After experimentally determining the propeller cavitation bucket, Vrijdag [33] has developed a control strategy that is aimed at maintaining the optimum inflow angle of the water onto the propeller blade, the angle of attack, near its optimum value. Experiments demonstrate the effectiveness of this strategy in the $\alpha_{eff} - \sigma_n$ phase plane, which will be referred to as a cavitation plot in the remainder of this paper. This effective angle of attack α_{eff}, is defined as follows:

$$\alpha_{eff}(t) = \arctan\left(\frac{P_{pd}(t)}{0.7\pi}\right) - \arctan\left(\frac{c_1 v_a(t)}{0.7\pi n_p(t) D_p}\right) - \alpha_i, \tag{25}$$

where α_i is the shock free entry angle onto the leading edge of the propeller profile in deg, and c_1 is the coefficient to calibrate the effective angle of attack with the centre point of the cavitation bucket such that

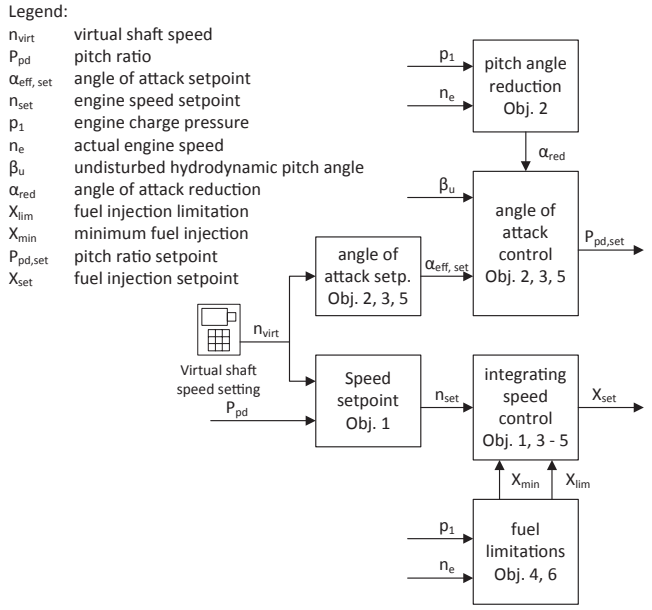

Fig. 8. Schematic representation of proposed adaptive pitch control strategy for diesel mechanical propulsion with CPP.

the cavitation bucket can be represented as two lines in the α_{eff}–σ_n phase plane. Vrijdag [33, Ch. 7 pp. 115–120] describes the procedure to determine c_1 and Vrijdag [33, Ch. 7 pp. 147–159] describes the schematic cavitation bucket in the α_{eff}–σ_n phase plane, with the cavitation number σ_n defined as follows:

$$\sigma_n(t) = \frac{p_\infty - p_v}{1/2\rho_{sw}(n_p(t))^2 D_p^2}, \tag{26}$$

where p_∞ is the ambient water pressure at the center-line of the propeller in Pa, p_v is the vapour pressure of water at the ambient temperature in Pa, ρ_{sw} is seawater density in kg/m^3, and D_p is the propeller diameter in m.

The proposed control strategy forms the basis for the control strategy proposed in this paper. While the implementation of the angle off attack strategy in [33] was aimed at minimising cavitation, the work already concluded that this control strategy improves acceleration behaviour and prevents the loss of ship speed due to pitch reduction when preventing engine loading. This study aims to quantify the benefits of the adaptive pitch control strategy and proposes an integrated control strategy aimed at achieving all control objectives mentioned above. The angle of attack setpoint $\alpha_{eff,set}$ can be defined as a function of the virtual shaft speed, but in this case is taken constant and determines the normalised pitch control setpoint $P^*_{pd,set}$, as follows:

$$P^*_{pd,set}(t) = \frac{0.7\pi\tan(\theta_{set}(t) - \theta_{red}(t)) + P_{pd,0}}{P_{pd,nom} - P_{pd,0}} \tag{27}$$

$$\theta_{set}(t) = \alpha_{eff,set} + \alpha_i + \arctan(c_1\tan(\beta(t))) \tag{28}$$

$$\beta(t) = arctan\left(\frac{v_a(t)}{0.7\pi n_p(t) D_p}\right) \tag{29}$$

$$v_a(t) = v_s(t)(1 - f_w) + v_w(t), \tag{30}$$

where θ_{set} is the pitch angle setpoint in rad, θ_{red} is the pitch angle setpoint reduction in rad, β is the hydrodynamic pitch angle in rad, v_a is the advance speed of the water relative to the propeller in m/s, and f_w is the wake fraction, which is considered constant.

While the actual hydrodynamic pitch angle cannot be directly measured, we assume this value is available. In [33] a method is proposed to derive the hydrodynamic pitch angle by measuring thrust and using the inverse of the four quadrant open water diagram. Moreover, a pitch angle reduction term θ_{red} is added, which is proportional to the margin of the unlimited fuel injection setpoint to the fuel injection limitations, as follows:

$$\theta_{red}(t) = P_\theta X_{mar}(t) \tag{31}$$

$$0 \leqslant \theta_{red}(t) \leqslant \theta_{red,max}, \tag{32}$$

where P_θ is the proportional pitch angle reduction gain, X_{mar} is the fuel injection margin as defined in (39) and $\theta_{red,max}$ indicates the maximum value of the pitch angle reduction.

When the control objective to minimise acceleration time is also strived for, the air excess ratio limitation of the engine causes pitch reduction. Subsequently, the angle of attack is not maintained at its optimum value. In a separate low cavitation mode the air excess ratio limitation is prevented by limiting the fuel injection increase rate limitation, $R_{X,cav}$.

3.1.3. Minimise fuel consumption

The operating points of four components determine the fuel consumption of a direct mechanical propulsion plant with controllable pitch propeller: the diesel engine, the gearbox, the shaft-line and the propeller. The speed and fuel injection of the diesel engine, in combination with the charge pressure, determine the specific fuel consumption of the engine. The speed and torque of the shaft-line and gearbox determine their losses, which are relatively small and will not be considered for the control strategy. Finally, the propeller open water efficiency is determined by the operating point of the propeller, governed by ship speed, wake-field disturbance from waves and propeller speed and pitch. Moreover, automotive and maritime research has shown that quasi static behaviour to a large extent determines the fuel consumption of cars and ships [75–77], although Blanke et al. [48] have demonstrated the engine control strategy can utilise the varying inflow velocity to increase the propeller efficiency in moderate seas, as will be addressed in Section 3.1.4.

The operating point at which the diesel engine consumes the minimum amount of fuel for a given power can be established from the specific fuel consumption contour plot, shown for the case study diesel engine in Fig. 9. At the lowest fuel consumption for a given power, the gradient of the specific fuel consumption is zero. The theoretical cube law propeller curve with a design point at full speed at 90% of rated power is also shown in Fig. 9. On this propeller curve, the fuel consumption is very close to its lowest value for a give power, as the gradient of the specific fuel consumption is close to zero. Moreover, the diesel engine project guide recommends operating the diesel engine on

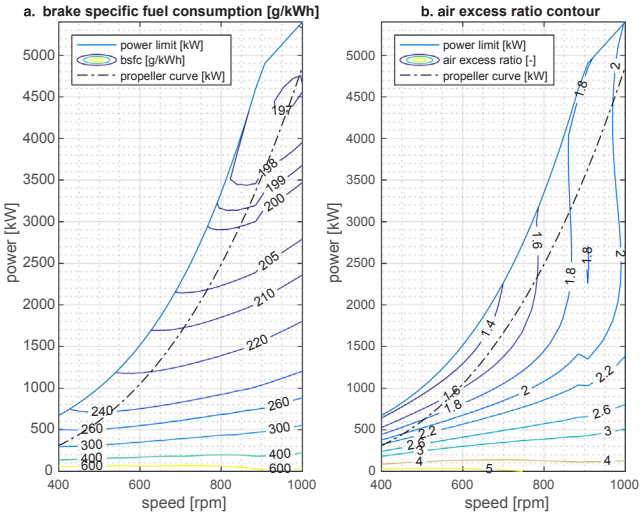

Fig. 9. Specific fuel consumption and air excess ratio contour plot in engine operating envelope with theoretical cube law propeller curve.

this propeller curve, as the margin to the engines power limit is sufficient [78].

Similarly, the control objective to operate the engine at or close to the operating point defined by the theoretical propeller curve also leads to the highest possible open water efficiency of the propeller, as the open water efficiency typically is highest at the highest possible pitch and the operating envelope of the engine does not allow increasing pitch, and thus the load, above the theoretical propeller curve. For engines with wide operating envelopes, alternative control strategies might lead to lower fuel consumption. One such strategy can reduce fuel consumption in part load by up to 7%, by using hybrid propulsion with power take-off for a sequentially turbocharged diesel engine, as discussed in [79]. In conclusion, the second resulting control objective is to operate the engine at or close to the operating point defined by the theoretical propeller curve with a design point at 90% rated power.

This control objective can be achieved by governing control action propeller pitch ratio setpoint $P_{p,set}$ and can be translated in maintaining a constant propeller torque coefficient K_Q, which is defined as [25]:

$$K_Q(t) = \frac{Q_p(t)}{\rho_{sw}(n_p(t))^2 D_p^4}, \tag{33}$$

where Q_p is the open water propeller torque in kNm, and D_p is the propeller diameter in m. However, control objectives 3, 4 and 6 benefit from maintaining a constant effective angle of attack α_{eff}, instead of a constant pitch or propeller torque coefficient K_Q. Moreover, for the case study Patrol Vessel, with a nearly cubed resistance curve due to its low Froude number, maintaining a constant angle of attack also leads to operating the propeller at an almost constant propeller torque coefficient K_Q and at or close to the theoretical propeller curve. Therefore, the propeller pitch ratio setpoint $P_{p,set}$ is controlled to maintain the angle of attack at its setpoint value $\alpha_{eff,set}$, as defined in (27) and (28).

3.1.4. Maintain engine air excess ratio

The engine air excess ratio, the relative amount of air that is left after complete combustion of all fuel, is an important indicator for engine thermal loading, as demonstrated in [80,81,56,24], and Figs. 9 and 10. While the air excess ratio contour plot in Fig. 9 illustrates the air excess ratio in stationary conditions, the air excess ratio during dynamic conditions, such as acceleration and wave induced disturbances, can be significantly lower or higher due to the turbocharger lag. In this section, we will first address wave induced disturbances and propose integrating speed control to resolve these and then propose a fuel injection constraint that maintains the air excess ratio at a minimum value during acceleration.

Geertsma et al. [50] have demonstrated that engine torque control as opposed to engine speed control can completely eliminate thermal loading fluctuation due to disturbance from waves. Moreover, Blanke et al. [48] have demonstrated with model experiments that torque control can lead to 2% fuel consumption reduction in moderate seas by utilising the varying inflow velocity onto the propeller blade, thus increasing the propeller efficiency. However, the first control objective is to provide the requested virtual shaft speed and torque control would require an additional torque sensor, that might be less reliable than speed sensing. Therefore, we propose to use integrating speed control, without a proportional gain on the speed error, similar to the slow integrating speed control strategy that Rubis and Harper [82] proposed for gas turbine mechanical propulsion, due to its good performance in heavy waves. Slow integrating speed control exhibits a similar dynamic behaviour in waves as torque control and, in combination with (24), also provides the requested virtual shaft speed. Thus, the following control algorithm is proposed to achieve slow integrating speed control:

$$X_I(t) = K_{I,ic} \int_0^t \left(\frac{n_{set}(t) i_{gb}}{n_{e,nom}} - \frac{n_e(t)}{n_{e,nom}} \right) dt, \tag{34}$$

where X_I is the fuel injection setpoint from integrating speed control, $K_{I,ic}$ is the reset rate for slow integrating speed control, i_{gb} is the gearbox reduction ratio, and $n_{e,nom}$ is the nominal engine speed in Hz.

During an acceleration, the charge pressure will lag at a lower value due to the turbocharger inertia, which causes a higher thermal loading than in stationary conditions. In order to prevent thermal overloading, the objective thus is to maintain the air excess ratio at a minimum value. This can be achieved by first limiting the fuel pump position based on the charge pressure and secondly reducing the angle of attack setpoint when the fuel pump position is limited. The fuel pump position limitation is defined as follows, as derived from [24, Eqs. (4) and (5)]:

$$X_{lim,\lambda}(t) = \frac{p_1(t) V_1}{R_a T_1 \sigma_f m_{f,nom} \lambda_{min}}, \tag{35}$$

where $X_{lim,\lambda}$ is the fuel injection limitation to limit the air excess ratio λ in % of nominal fuel injection $m_{f,nom}$, V_1 is the cylinder volume at the start of compression in m^3, R_a is the gas constant of air in J/kg K, T_1 is the temperature at the start of compression in K and σ_f is the stoichiometric air fuel ratio of the fuel.

Another important parameter to limit engine thermal loading is the rate of increase of exhaust valve temperature dT_{ev}/dt during an acceleration, which is mainly determined by the rate of increase of torque and therefore fuel injection X. In order to limit this rate of increase, the proposed adaptive pitch control strategy incorporates a fuel injection increase rate limitation $R_{X,therm}$ to prevent thermal overloading due to a high dT/dt. Moreover, in order to prevent cavitation due to running into the air excess ratio limitation, a second setting for this rate is determined for the low cavitation mode: the torque increase rate limitation for reduced cavitation $R_{X,cav}$.

3.1.5. Minimise acceleration time

The objective to minimise acceleration time is restricted by the objective to prevent engine thermal overloading [38] and thus by the objective to maintain engine air excess ratio. In traditional control strategies this is achieved by limiting the rate of the increase in engine speed during an acceleration manoeuvre, as demonstrated in [50,21].Vrijdag [31] has demonstrated, through a combination of simulation and validation, that the acceleration behaviour improves due to the proposed angle of attack control strategy with an acceptable engine thermal loading. In essence, the acceleration manoeuvre is faster, because the pitch is increased more slowly during the acceleration manoeuvre, leading to higher engine speed. Geertsma et al. [24] have demonstrated that indeed a reduced pitch during an acceleration manoeuvre increases engine speed and reduces engine thermal loading,

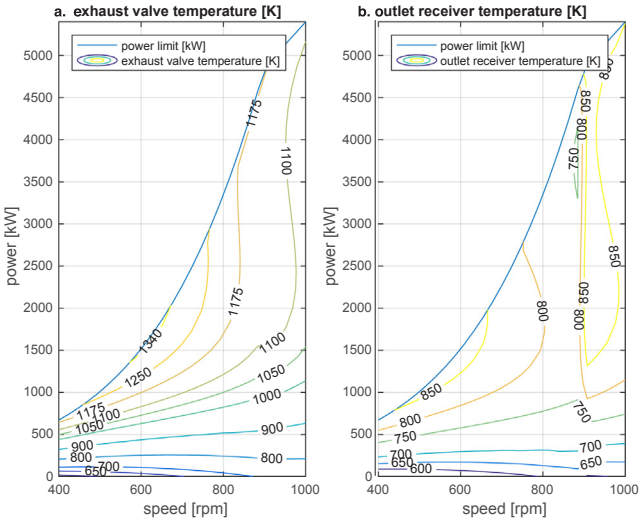

Fig. 10. Exhaust valve and receiver temperature plot in engine operating envelope with theoretical cube law propeller curve.

because the turbo charger pressure and thus the air excess ratio increases faster at higher engine speeds. In the proposed slow integrating speed control strategy, according to (34), speed increase rate limiters are not required, as will be demonstrated in the results of this paper. Therefore, the setting of the reset rate K_I determines the speed of acceleration and needs to be determined in a trade-off between acceleration behaviour and engine thermal loading during an acceleration.

3.1.6. Prevent engine overspeed and under-speed

Slow integrating speed control as defined in (34) introduces the risk of engine overspeed or under-speed due to disturbances, as integrating speed control follows the speed setpoint significantly slower than an aggressive PI controller. To prevent engine overspeed, the following fuel limitation is introduced:

$$X_{\text{lim,os}}(t) = \frac{n_{\text{e,max}} - n_{\text{e}}(t)}{n_{\text{e,nom}}} P_{\text{os}}, \tag{36}$$

where $X_{\text{lim,os}}$ is the fuel injection limitation to prevent overspeed, $n_{\text{e,max}}$ is maximum engine speed, and P_{os} is the overspeed limitation gain. Similarly, the following minimum fuel injection X_{min} prevents engine under-speed:

$$X_{\text{min}}(t) = \frac{n_{\text{e,min}} - n_{\text{e}}(t)}{n_{\text{e,nom}}} P_{\text{us}}, \tag{37}$$

where $n_{\text{e,min}}$ is minimum engine speed, and P_{us} is the under-speed limitation gain. Moreover, the fuel injection limitation and the fuel injection margin X_{mar} are defined as:

$$X_{\text{lim}}(t) = \max(X_{\text{lim,os}}(t), X_{\text{lim},\lambda}(t)) \tag{38}$$

$$X_{\text{mar}}(t) = X_{\text{I}}(t) - X_{\text{lim}}(t). , \tag{39}$$

where X_{lim} is the fuel injection limitation in %. Finally, the fuel injection is limited between the minimum fuel injection X_{min} and the fuel injection limitation X_{lim}, as follows:

$$X_{\text{I}}(t) < X_{\text{min}}: X_{set}(t) = X_{\text{min}} \tag{40}$$

$$X_{\text{min}}(t) \leqslant X_{\text{I}}(t) \leqslant X_{lim}(t): X_{set}(t) = X_{\text{I}}(t) \tag{41}$$

$$X_{\text{I}}(t) > X_{lim}(t): X_{set}(t) = X_{lim}(t). \tag{42}$$

With a traditional combinator curve, reducing pitch at low speed settings while maintaining minimum engine speed prevents engine under-speed. When applying the adaptive pitch control strategy the pitch should also be constrained to the value associated with minimum engine speed, as follows:

$$P^*_{\text{pd,max}}(t) = \frac{n_{\text{virt,set}}(t) i_{\text{gb}}}{n_{\text{e,mins}}} \tag{43}$$

$$P_{\text{pd,set}}(t) = P_{\text{pd,0}} + \max(P^*_{\text{pd,max}}(t), P^*_{\text{pd,set}}(t))(P_{\text{pd,nom}} - P_{\text{pd,0}}), \tag{44}$$

where $n_{\text{e,mins}}$ is the minimum engine speed setpoint.

Finally, when pitch is limited to prevent engine under-speed, engine speed should be kept constant at minimum engine speed $n_{\text{e,min}}$. In this region, slow integrating speed control can lead to excessive speed fluctuation, which will be limited by the under-speed fuel injection limitation described in (37). Nevertheless, in this region engine speed is better kept constant by applying traditional fast PI speed control, as described in [24], as follows:

$$X_{PI}(t) = K_P \left(\frac{n_{ref}(t)}{100} - \frac{n_e(t)}{n_{e_{nom}}} \right) + K_I \int_0^t \left(\frac{n_{ref}(t)}{100} - \frac{n_e(t)}{n_{e_{nom}}} \right) dt, \tag{45}$$

where X_{PI} is the unlimited fuel injection setpoint for speed control, K_P is the proportional gain and K_I is the reset rate. PI speed control replaces slow integrating speed control when the engine speed setpoint is less or equal to minimum engine speed $n_{\text{e,min}}$ with a hysteresis of 2.5%. Effectively, PI gain scheduling [83] is applied in this case with a clear switching value, when the engine speed setpoint is at its minimum value with a hysteresis of 2.5% to prevent repetitious switching between the gain values. While repetitious switching is prevented by using the speed setpoint as switching variable, alternatively, a continuous function for the proportional gain P could be derived, as used in pitch control with gain scheduling for wind turbines [84].

3.2. Controller settings

With the traditional control strategy, many of the control parameters require extensive tuning [24,85,73, Section 3.3]. The resulting parameters of the traditional control strategy are listed in [24, Table 2-6]. Alternatively, the proposed control strategy primarily requires limitations for physical parameters and a number of gains. The only parameters that require tuning are the gain and reset rate for speed control at minimum engine speed $K_{\text{P,sc}}$ and $K_{\text{I,sc}}$, and the reset rate for slow integrating speed control $K_{\text{I,ic}}$.

Various tuning strategies for PI control are discussed in literature [83,86–88]. While Aström and Häggelund [83] provide an overview of tuning strategies, Xiros [86] proposes an improved PID tuning method for marine engine speed regulation to meet sensitivity H_∞ requirements. However, the stability of the system does not require stringent engine speed disturbance rejection criteria, as demonstrated in [50] and we aim to minimise torque fluctuations. Moreover, the reset rate for slow integrating speed control $K_{\text{I,ic}}$ physically primarily influences the rate of temperature increase dT_{ev}/dt during an acceleration and therefore is tuned to achieve gradual dT_{ev}/dt. Moreover, the influence of the gain and reset rate for speed control K_{p} & K_{i} on the behaviour in waves can be investigated with linearised propulsion system models as proposed in [87,88]. The parameters in this paper were based on this approach and the results in this paper demonstrate the stability of the used settings. The resulting control parameters for the proposed adaptive pitch control strategy are listed in Table 1.

4. Results

4.1. Simulation experiments

The simulation experiments for the case study *Holland* class Patrol Vessel in this paper aim to compare the proposed control strategy with the baseline control strategy of the actual vessel, which has been used for the validation of the simulation model in [24]. We use two types of straight line manoeuvres to establish the Measures of Performance (MOP): sailing at constant speed and two acceleration manoeuvres. First, the slam start manoeuvre proposed in [89] is used to establish the shortest possible acceleration time from 0 kts to 15 kts ship speed, by setting the virtual shaft speed to the maximum value at the start of the manoeuvre. Second, intermediate sprints are used to establish MOPs during regular acceleration. For intermediate sprints, the virtual shaft speed setting is increased from the setting that provides the starting

Table 1
Control parameters for the proposed adaptive pitch control strategy.

Control parameter	Value
Effective angle of attack setpoint $\alpha_{\text{eff,set}}$ in deg	10.5
Reset rate slow integrating speed control $K_{\text{I,ic}}$	0.2
Proportional gain speed control $K_{\text{P,sc}}$	2
Reset rate speed control $K_{\text{I,sc}}$	0.5
Minimum engine speed $n_{\text{e,min}}$	350 rpm
Maximum engine speed $n_{\text{e,max}}$	1050 rpm
Under-speed limitation gain P_{us}	8
Overspeed limitation gain P_{os}	22
Fuel injection rate for thermal loading $R_{\text{X,thermal}}$	1.67%
Fuel injection rate for cavitation $R_{\text{X,cav}}$ in %	0.42%
Conservative air excess ratio limitation λ_{min}	1.6
Regular air excess ratio limitation λ_{min}	1.45

Table 2
Hull and wave model parameters in trial and design conditions, from [24].

Condition	Trial	Design
Ship mass m in 10^3kg	3800	3800
Number of propellers m	2	2
Thrust deduction factor t	0.155	0.155
Propeller center depth z in m	6.5	6.5
Wave amplitude ζ in m	0	1
Wave frequency ω_{wv} in rad/s	–	0.966
Wave number k	–	0.095

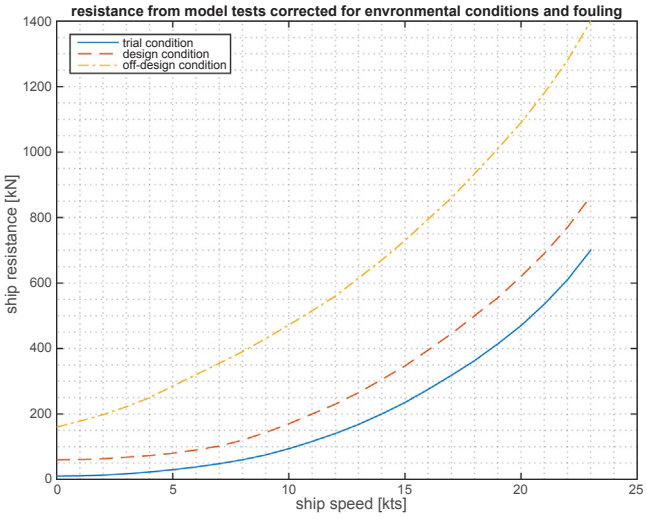

Fig. 11. Ship resistance from model tests corrected for environmental conditions and fouling in trial, design and off-design condition, from [24].

ship speed to the setting that achieves the speed at the end of the manoeuvre. These benchmark manoeuvres can be used to demonstrate that the proposed control strategy meets the objectives described in Section 3.1. Moreover, we have performed the proposed benchmark manoeuvres to establish the Measures of Performance (MOPs) proposed in [24].

As reported in [24], 'the ship resistance and the wave model parameters very strongly depend on the conditions in which the ship operates'. In this study, we consider the following two typical conditions:

- Trial condition, defined as Sea State 0, wind speed of 3 m/s and no fouling.
- Design condition, defined as Sea State 4, wind speed of 11 m/s, head seas and wind and 6 months out of dock fouling.

The parameters that represent these conditions are shown in Table 2 and Fig. 11, from [24].

The simulation results have been obtained with MATLAB Simulink R2016b software on a PC with Intel Core i7 processor and 16 GB memory. The simulation to establish the slam start and intermediate

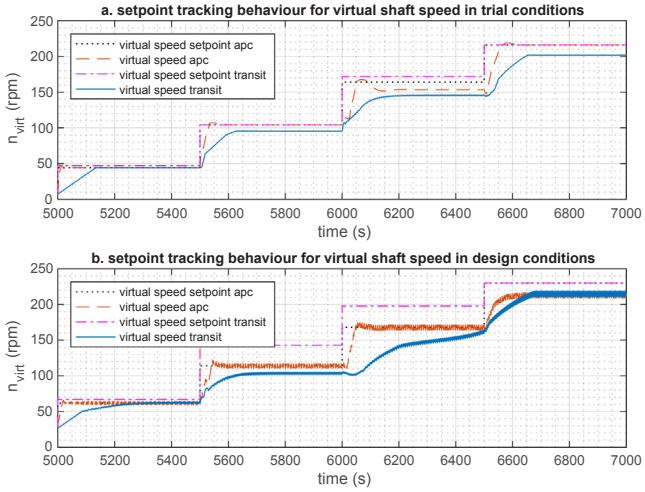

Fig. 12. Setpoint tracking behaviour for virtual shaft speed in trial and design conditions for baseline transit control and adaptive pitch control with limited air excess ratio.

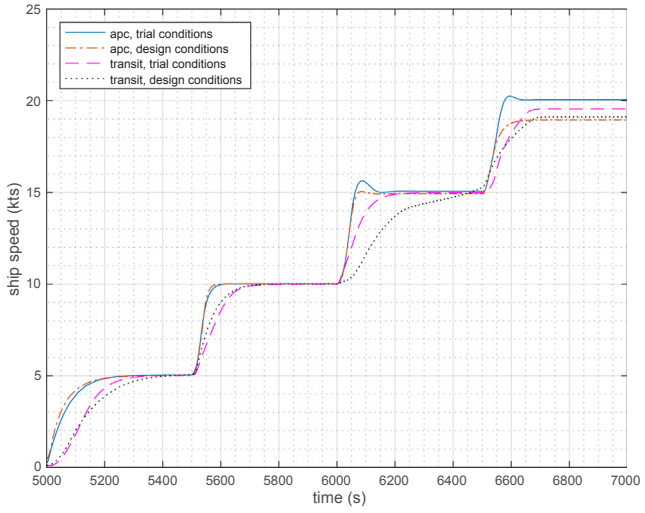

Fig. 13. Ship speed during intermediate sprint acceleration in trial and design conditions for baseline transit control and adaptive pitch control with limited air excess ratio.

sprint accelerations requires 6 s simulation time in trial conditions and 77 s in design conditions. Both these simulations cover 9000 s, or 2.5 h simulated time. The difference in simulation time is caused by the dynamics introduced by waves, limiting the maximum step time for design conditions. The simulation to establish the static operating point for design conditions over 22 virtual shaft speeds, allowing stabilisation of each operating point for 1000 s, takes 256 s for 22,000 s simulated time. In conclusion, the simulation requires approximately 1/100 s simulation time for 1s simulated time in design conditions.

Table 3
Control strategies, modes and settings evaluated in simulation experiments reported in Section 4.

Control strategy name	Mode	Increase rate R_{L+} or R_X	Air excess ratio λ_{min}
Baseline manoeuvre speed control	Manoeuvre	R_{L+} = 1.5%/s	
Baseline transit speed control	Transit	R_{L+} = 0.75%/s	
Adaptive pitch control (APC)	Fast APC	$R_{X,therm}$ = 1.67%/s	λ_{min} = 1.45
Adaptive pitch control (APC)	APC with limited air excess ratio λ	$R_{X,therm}$ = 1.67%/s	λ_{min} = 1.6
Adaptive pitch control (APC)	Slow APC to prevent cavitation	$R_{X,cav}$ = 0.42%/s	λ_{min} = 1.6

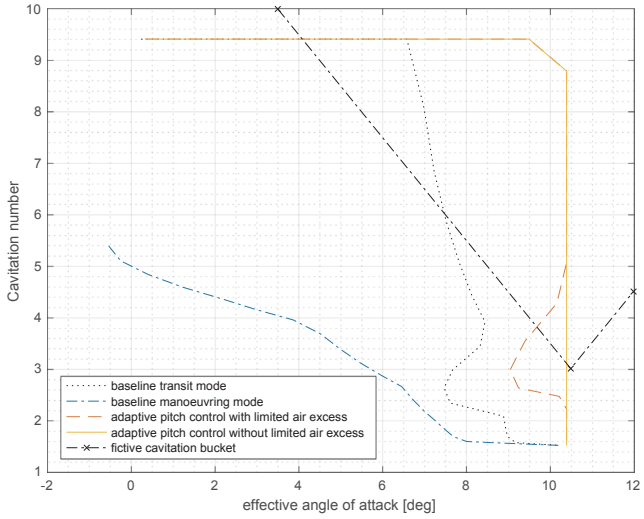

Fig. 14. Cavitation plot from low speed to maximum speed for trial conditions in manoeuvring and transit mode and with adaptive pitch control with and without limited air excess ratio.

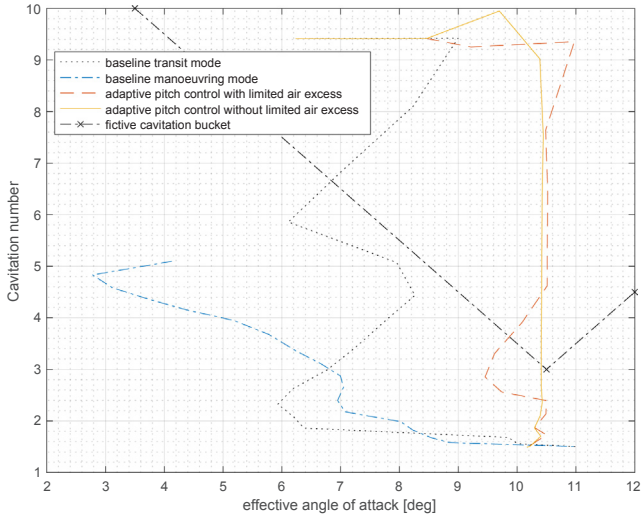

Fig. 15. Cavitation plot at constant speed from low speed to maximum speed for baseline transit and manoeuvre mode and for adaptive pitch control with (1.6) and without (1.45) limited air excess ratio in design conditions.

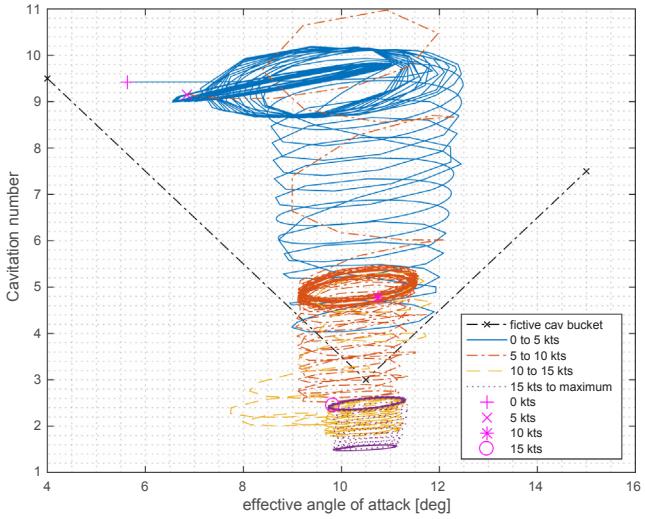

Fig. 16. Cavitation plot in design conditions during intermediate sprints from 0 to 5 kts, 5 to 10 kts, 10 to 15 kts, and 15 kts to maximum ship speed, for adaptive pitch control with limited air excess ratio (1.6) and a fuel injection increase rate to only prevent thermal overloading $R_{X,therm}$.

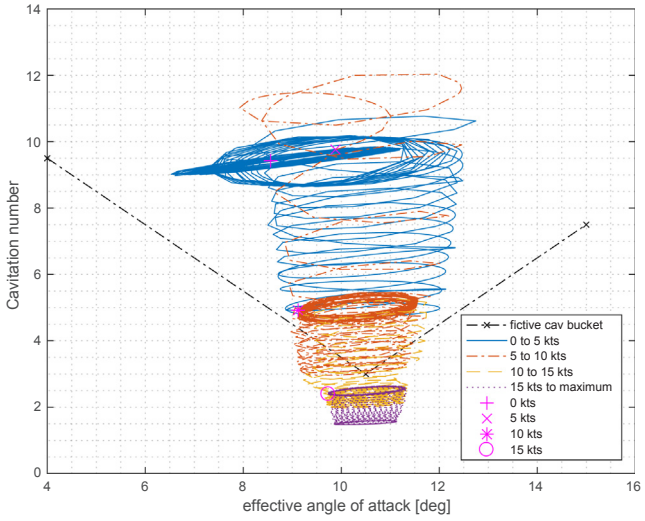

Fig. 17. Cavitation plot in design conditions during intermediate sprints from 0 to 5 kts, 5 to 10 kts, 10 to 15 kts, and 15 kts to maximum ship speed, for slow adaptive pitch control to prevent cavitation $R_{X,cav}$.

4.2. Evaluated control strategies

In the simulation experiments, the baseline transit and manoeuvre mode control strategies, as described in [24], are compared with the adaptive pitch control strategy as described in Section 3, with various settings as reported in Table 1. An overview of the 5 control strategies, their modes and settings used for the evaluation in Section 4 is listed in Table 3.

4.3. Evaluation of control objectives

4.3.1. Virtual shaft speed

The first control objective is to provide the requested virtual shaft speed. This objective is one of the key reasons to employ traditional speed control, as feedback control on speed can robustly handle the uncertainty associated with weather conditions, ships course relative to the wind and waves, hull fouling and ships displacement. Figs. 12 and 13 present the results of the intermediate acceleration from 0 kts to 5 kts, 5 kts to 10 kts, 10 kts to 15 kts and 15 kts to maximum speed for trial conditions and for design conditions, reflecting two very different conditions and thus the described uncertainty.

The baseline control strategy provides the requested shaft speed unless pitch is reduced to prevent overloading, as described in [24, Section 3.2, pp. 1618–1619]. While engine speed control robustly maintains engine speed at the requested speed from the combinator curve, the pitch reduction strategy reduces pitch and therefore virtual shaft speed. Therefore, in conditions with a high ship resistance, such as design conditions, the traditional control strategy does not actually provide the requested virtual shaft speed, as shown in Fig. 12. Actually, even in trial conditions, at certain engine speed the requested virtual shaft speed is not achieved. The operator can achieve the required ship speed by requesting a higher virtual shaft speed than the virtual shaft speed required for that ship speed, which is clearly demonstrated by the high virtual speed setpoint of 200 rpm required to achieve 15 kts ship speed with baseline transit control in design conditions in Fig. 12b.

The proposed adaptive pitch control strategy, in this case with limited air excess ratio, follows the virtual shaft speed setpoint

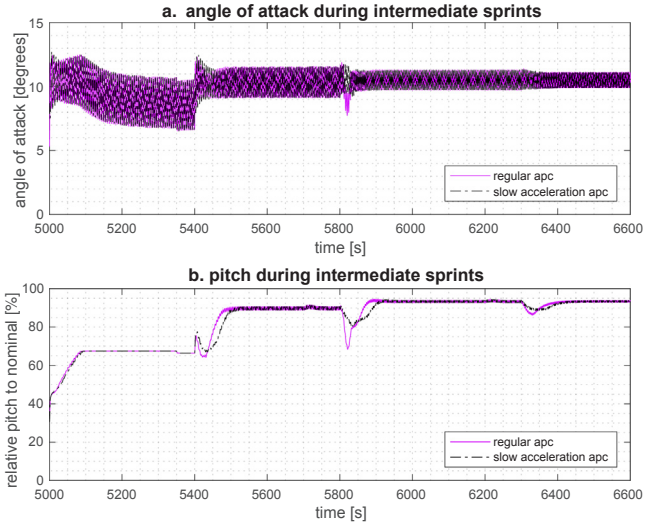

Fig. 18. Angle of attack and pitch during intermediate sprints in design conditions from 0 to 5 kts, 5 to 10 kts, 10 to 15 kts, and 15 kts to maximum ship speed comparing adaptive pitch control with limited air excess ratio (1.6) and fuel injection increase rate $R_{X,therm}$, with slow adaptive pitch control with fuel injection increase rate $R_{X,cav}$.

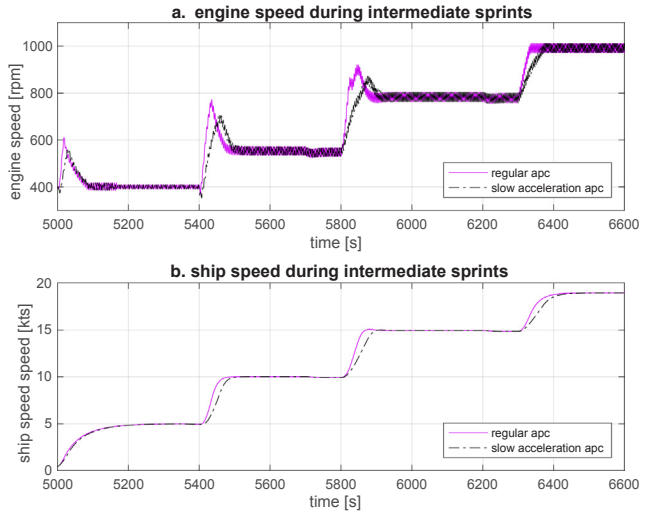

Fig. 19. Engine and ship speed during intermediate sprints in design conditions from 0 to 5 kts, 5 to 10 kts, 10 to 15 kts, and 15 kts to maximum ship speed comparing adaptive pitch control with limited air excess ratio (1.6) and fuel injection increase rate $R_{X,therm}$, with slow adaptive pitch control with fuel injection increase rate $R_{X,cav}$.

accurately, because higher or lower pitch than nominal pitch is compensated with a proportional decrease or increase in speed setpoint due to (24). Only if the air excess ratio limitation λ_{min} is higher than the air excess ratio on the theoretical propeller curve, for this engine higher than 1.50, the virtual shaft speed will not reach its setting as the air excess ratio limitation is not compensated by increased engine speed. Slow integrating speed control responds more slowly to changes in engine speed and therefore ship speed, leading to a slight overshoot in virtual shaft speed during acceleration, as shown in Fig. 12. However, this overshoot only leads to an overshoot in ship speed of 0.3 kts, and only in light trial conditions. During design conditions, when the engine margin is smaller, constant ship speed is only reached when the virtual shaft speed overshoot has already stabilised. Therefore, this overshoot is acceptable, also because it leads to significantly faster acceleration. The robust virtual shaft speed following capability under large uncertainties is a significant advantage of the proposed adaptive pitch

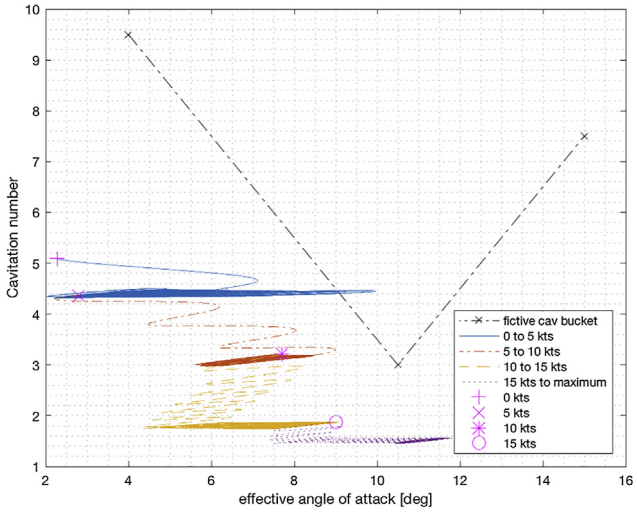

Fig. 20. Cavitation plot in design conditions during intermediate sprints from 0 to 5 kts, 5 to 10 kts, 10 to 15 kts, and 15 kts to maximum ship speed with baseline transit mode.

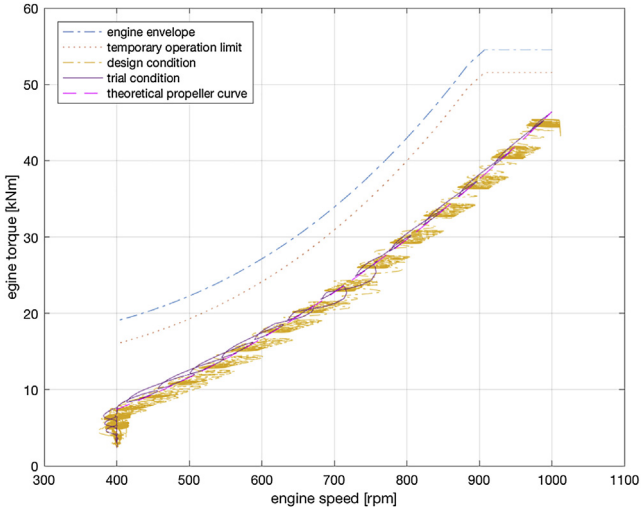

Fig. 21. Constant ship speed operation from low speed to maximum speed in engine operating envelope for fast adaptive pitch control strategy (with air excess ratio limitation $\lambda_{lim} = 1.45$) in trial and design conditions.

control compared to the baseline strategy, that does not accurately follow the virtual shaft speed setpoint, and this behaviour is achieved with simple feedback control as opposed to complex algorithms as proposed in [90].

4.3.2. Maintain operation within the cavitation bucket

While the propeller of the patrol vessel has not been designed for low noise operation, the angle of attack at the design point of the propeller is too high for low cavitation behaviour. However, for the evaluation of the control objective to maintain operation within the cavitation bucket, we assume the cavitation bucket is centred around the angle of attack at the design point, which could be achieved at a lower angle of attack with a similar propeller with a larger diameter. Therefore, the objective of the control strategy is to maintain the angle of attack centred around the design angle of attack: 10.5 deg.

The cavitation plots at constant speed for trial and design conditions in Figs. 14 and 15 demonstrate that the adaptive pitch control strategy maintains the effective angle of attack at the desired angle of 10.5 degrees, irrespective of the uncertainties in weather conditions, while the effective angle of attack of the baseline transit and manoeuvre mode

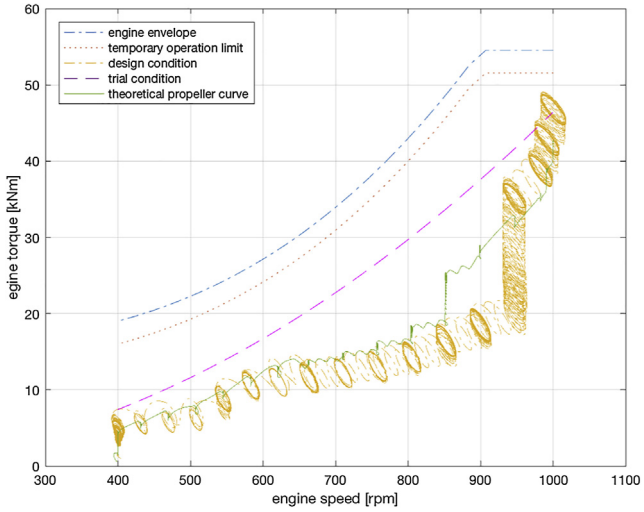

Fig. 22. Constant ship speed operation from low speed to maximum speed in engine operating envelope for baseline transit control strategy in trial and design conditions.

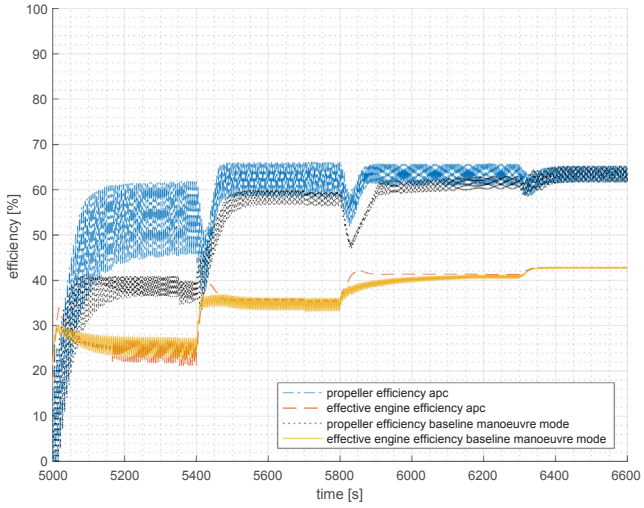

Fig. 23. Propeller open water efficiency and effective engine efficiency during intermediate accelerations from 0 to 5 kts, 5 to 10 kts, 10 to 15 kts, and 15 kts to maximum ship speed in design conditions for baseline manoeuvre mode and adaptive pitch control.

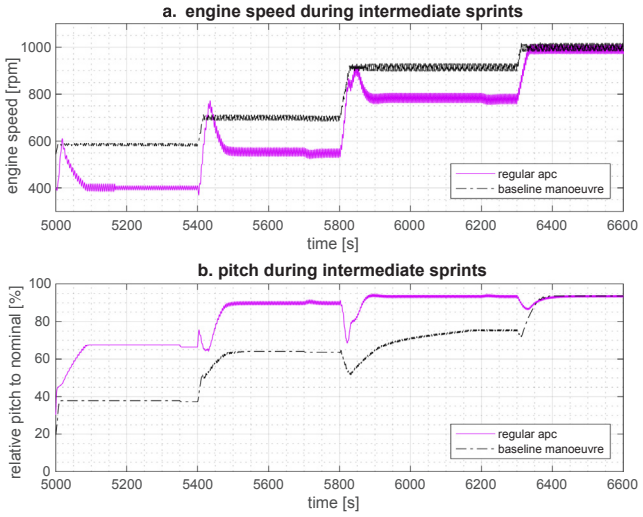

Fig. 24. Engine speed and pitch during intermediate accelerations from 0 to 5 kts, 5 to 10 kts, 10 to 15 kts, and 15 kts to maximum ship speed in design conditions for baseline manoeuvre mode and fast adaptive pitch control.

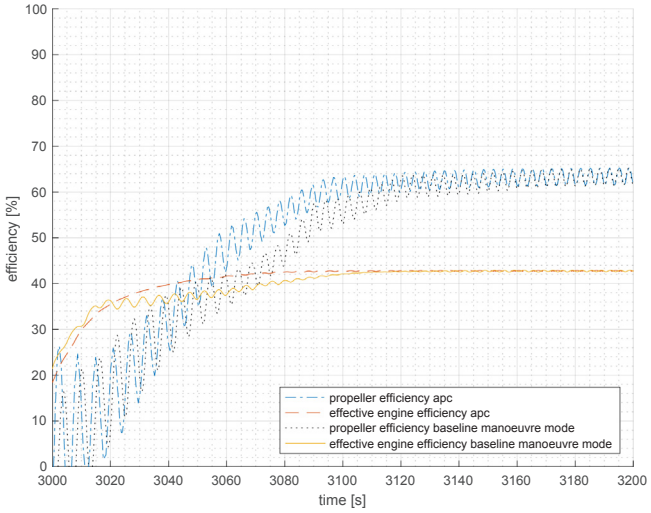

Fig. 25. Propeller open water efficiency and effective engine efficiency during slam start acceleration from 0 kts to maximum ship speed in design conditions for baseline manoeuvre mode and fast adaptive pitch control.

strongly depends on weather conditions and is not kept constant for varying ship speed. Moreover, during intermediate sprints, shown in the cavitation plots in Figs. 16 and 17, the effective angle of attack is maintained centred around the desired value of 10.5, as opposed to the baseline transit mode plot shown in Fig. 20. The fluctuation in angle of attack, caused by waves, does not increase with the adaptive pitch control strategy compared to the fluctuation in angle of attack with a constant pitch angle in the baseline control strategies, confirming the adaptive pitch control strategy does not lead to instability.

However, the adaptive pitch control strategy with limited air excess ratio during acceleration does reduce pitch during the acceleration, as shown in Fig. 18 and then the angle of attack reduces during the manoeuvre, as shown in Fig. 16. This can be resolved by reducing the fuel injection increase rate to a lower value, $R_{X,cav}$. Then the pitch reduces only to maintain the angle of attack centred around 10.5 deg as shown in Figs. 18 and 17, leading to a lower rate of increase of engine speed and slower acceleration as shown in Fig. 19.

4.3.3. *Minimise fuel consumption*

The control objective to minimise fuel consumption during constant speed sailing is achieved when the engine runs on the theoretical propeller curve as argued in Section 3.1.3. The fast adaptive pitch control strategy achieves operating points and ellipses on the theoretical propeller curve at various ship speeds for transit and design conditions, as shown in Fig. 21. Alternatively, in Fig. 22 the baseline transit control strategy operates well below the theoretical propeller curve, mainly due to its conservative settings to prevent engine overloading under any circumstances [24, Section 3.3, p. 1619]. Moreover, the baseline transit control strategy operates further away from the theoretical propeller curve during design conditions than during trial conditions. The orientation of the ellipses due to speed and torque fluctuation from waves changes due to slow integrating speed control: the torque fluctuations reduce to minimal values at the cost of a slight increase in speed fluctuations, as shown in Fig. 21, compared to the more vertical ellipses in Fig. 22, almost eliminating fluctuating air excess ratio and temperatures as shown in Fig. 28. Thus, we can conclude the adaptive pitch control strategy at constant ship speed compensates the uncertainty in weather conditions robustly and runs the engine at its most efficient operating

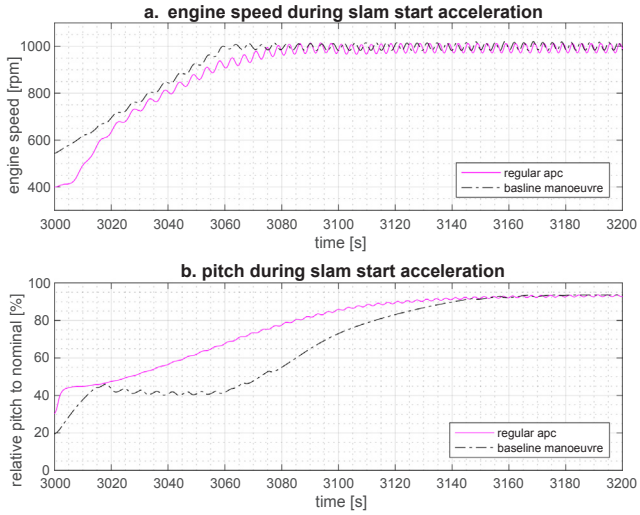

Fig. 26. Engine speed and pitch during slam start acceleration from 0 kts to maximum ship speed in design conditions for baseline manoeuvre mode and fast adaptive pitch control.

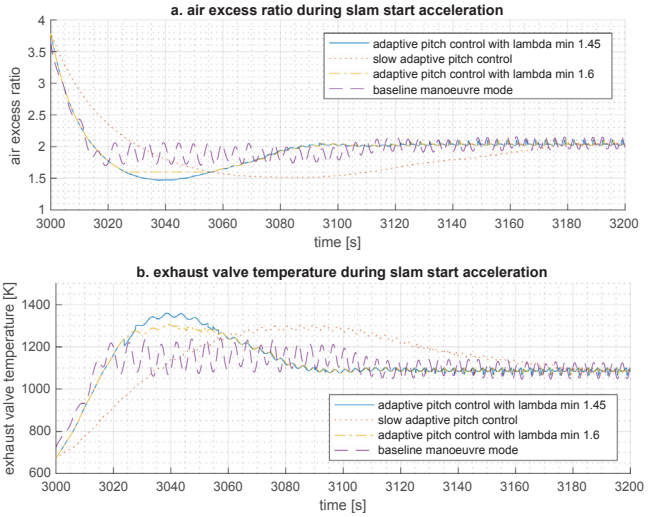

Fig. 27. Air excess ratio and exhaust valve temperature during slam start acceleration from stationary to maximum speed for adaptive pitch control strategy with various settings and baseline manoeuvre mode in design conditions.

point with sufficient margin to the engine operating envelope.

While the efficiency during acceleration does not heavily impact the fuel consumption over the operating profile of the ship, the efficiency during acceleration is also an indicator for acceleration performance. Therefore, Figs. 23 and 25 present the propeller open water efficiency and the effective engine efficiency during intermediate sprints and the slam start acceleration. During these accelerations, the engine efficiency and propeller efficiency are consistently higher for the fast adaptive pitch control strategy than for the baseline manoeuvre strategy. This has two reasons: first, the pitch in adaptive pitch control is higher and therefore the propeller operates at a higher open water efficiency; secondly, engine speed and engine load increase faster during acceleration, thus operating the engine at higher efficiency, because the adaptive pitch control strategy retracts pitch during the acceleration procedure to maintain the effective angle of attack as shown in Figs. 24 and 26.

The approach to minimise fuel consumption works very well with the proposed angle of attack approach, because fuel consumption is close to its minimum for a constant angle of attack for this particular engine. Nevertheless, if an engine has a different specific fuel consumption plot or if the trade-off between quasi-static NO_x emissions and fuel consumption should be taken into account, still an optimum quasi-static relationship between engine speed and torque could be established, which can be either translated into a relationship between shaft speed n_p and effective angle of attack α_{eff} or shaft speed n_p and propeller torque coefficient K_Q. The input for the development of the setting for this approach are static specific fuel consumption or NO_x emission maps, such as Fig. 9, Fig. 4 in [21], or Fig. 1 to 3 in [91]. Nuesch et al. [91] practically demonstrate NO_x emissions can be addressed with a quasi-static approach, as opposed to particulate matter (PM) emissions, which are sensitive to turbo charger lag and primarily benefit from a smooth torque trajectory, one of the benefits of the proposed slow integrating speed control strategy. Moreover, the static PM emission map in Fig. 2, in [91], shows that PM emissions for that specific automotive diesel engine appears near its minimum around the theoretical propeller curve. Therefore, future work could be aimed at confirming the expectation that the proposed adaptive pitch control strategy with slow integrating torque control also has a positive influence on PM emissions, and at investigating the trade-off between fuel consumption and NO_x emissions.

4.3.4. Maintain engine air excess ratio

Figs. 27 and 28 demonstrate that the proposed control strategy maintains the air excess ratio within the predefined limits, either above the minimum value of 1.45 or above the value of 1.6. When the air excess ratio λ_{min} is kept at a higher value, the temperatures during the slam start and intermediate acceleration are significantly lower. The baseline manoeuvre mode maintains even higher air excess ratios during all manoeuvres and therefore maintains lower temperatures, but that is caused by the very conservative settings to prevent overloading in heavy off-design conditions. In the nominal operating point on the theoretical propeller curve at 700 rpm and 1650 kW, the air excess ratio also is 1.35 and the exhaust valve temperature 1350 K. Therefore, an air excess ratio of 1.45 and an exhaust valve temperature of 1350 K does not lead to engine thermal overloading.

In almost all manoeuvres the maximum exhaust valve temperature remains below 1350 K, suggesting that the proposed control strategy with a minimum air excess ratio does not lead to thermal overloading. However, during the intermediate sprint from 10 to 15 kts the maximum cylinder temperature peaks to 1400 K, while the air excess ratio λ is maintained at a minimum value of 1.45. During this acceleration, engine speed ranges from 600 to 800 rpm, the range in which the air excess ratio is lowest and exhaust valve temperature highest during static conditions. Nevertheless, the higher temperature during this manoeuvre compared to other manoeuvres with the same minimum air excess ratio proves that the exhaust valve temperature is not directly dependant on the in-cylinder air excess ratio λ.

Close inspection of the simulation results shows that during this acceleration, the charge pressure lags, causing a reduced scavenge flow and therefore reduced exhaust valve cooling. This dependency of scavenge flow on charge pressure is clear from Eq. (29) and (30) in [24] and the relationship between scavenge flow and exhaust temperature is expressed in Eq. (51) in [24]. While further research would be required to establish whether this would indeed lead to thermal overloading of the engine, an alternative maximum fuel injection value as a function of charge pressure p_1 slightly more conservative than (35), could be used to reduce thermal loading during this specific case. Then, the relationship would either have to be experimentally established or have to be determined with the simulation model used in this study using the engine model in isolation and fixing the charge pressure model input.

Alongside the maximum temperature that is reached during acceleration, the rate of change of the exhaust valve temperature dT_{ev}/dt during an acceleration is also important for thermal stresses in the engine. Figs. 27 and 28 illustrate that for the adaptive pitch control strategy the average rate of change of the exhaust valve temperature

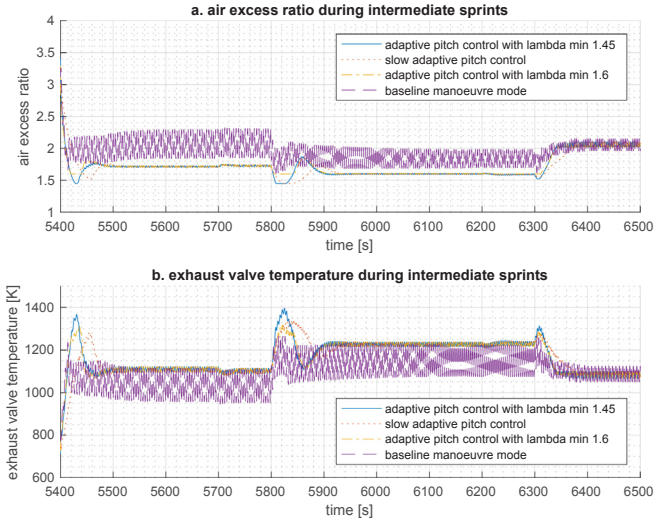

Fig. 28. Air excess ratio and exhaust valve temperature during intermediate sprints from 0 to 5 kts, 5 to 10 kts, 10 to 15 kts and 15 kts to maximum speed for adaptive pitch control strategy with various settings and baseline manoeuvre mode in design conditions.

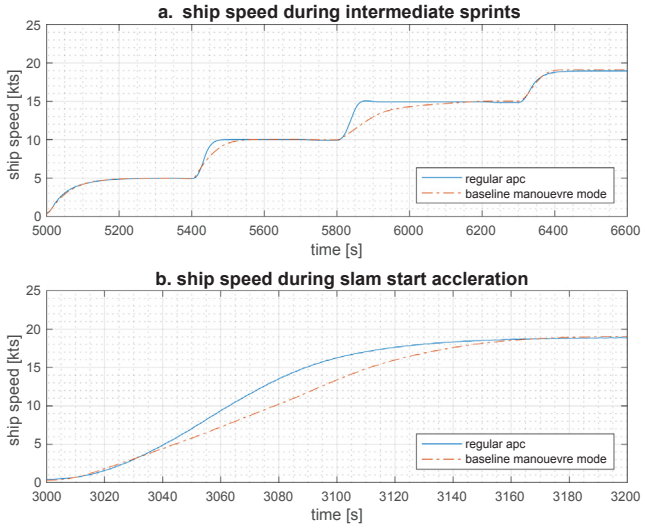

Fig. 30. Ship speed during intermediate sprints from 0 to 5 kts, 5 to 10 kts, 10 to 15 kts, and 15 kts to maximum ship speed and slam start acceleration for baseline manoeuvre control strategy and adaptive pitch control strategy (apc) in design conditions.

dT_{ev}/dt during the initial phase of the acceleration is similar to the baseline manoeuvre mode, but that the fluctuation due to waves does not occur for the adaptive pitch control strategy, due to the slow integration speed control. Moreover, close to the peak temperature, when the thermal stresses are highest, the increase rate of the temperature reduces, again without the fluctuation due to waves. While further research would be necessary to accurately determine the thermal stresses caused by the two control strategies, Figs. 27 and 28 suggest the behaviour of the adaptive pitch control strategy is more gradual and therefore less likely to cause thermal overloading.

4.3.5. Minimise acceleration time

The control objective to minimise acceleration time is a trade-off with the control objective to prevent engine thermal overloading. In order to reduce engine thermal loading during an acceleration manoeuvre, charge pressure needs to increase as fast as possible as a higher charge pressure provides a higher air excess ratio and scavenge flow increases at higher charge pressures. Increasing charge pressure during an acceleration can be best achieved by increasing engine speed and thus air flow in the engine. However, the fuel injection limitation of the baseline control strategy and the air excess ratio limitation of the proposed strategy limit the fuel injection during the acceleration manoeuvre and therefore the torque available for acceleration. Reducing pitch during the acceleration manoeuvre, which is an indirect effect of the effective angle of attack control strategy, helps increasing engine speed during an acceleration manoeuvre due to (1).

Fig. 24 demonstrates how, with fast adaptive pitch control, engine speed is increased during intermediate sprints due to pitch reduction, well above the engine speed after reaching constant speed, and Fig. 29 shows that this engine speed increase leads to a faster increase in charge pressure than during an intermediate sprint with the baseline manoeuvre mode. During a slam start acceleration with adaptive pitch control, engine speed and charge pressure do rise faster than with the baseline manoeuvre mode, but the increase in engine speed then is limited by the air excess ratio limitations due to the turbocharge lag, as

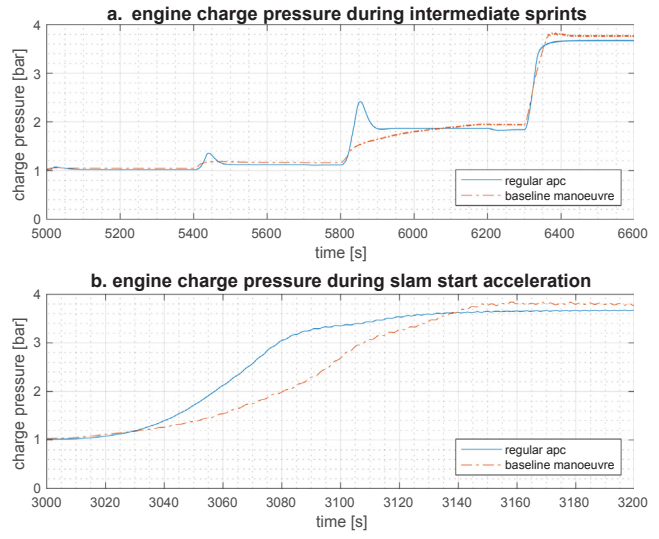

Fig. 29. Charge air during intermediate sprints from 0 to 5 kts, 5 to 10 kts, 10 to 15 kts, and 15 kts to maximum ship speed and slam start acceleration for baseline manoeuvre control strategy and adaptive pitch control strategy (apc) in design conditions.

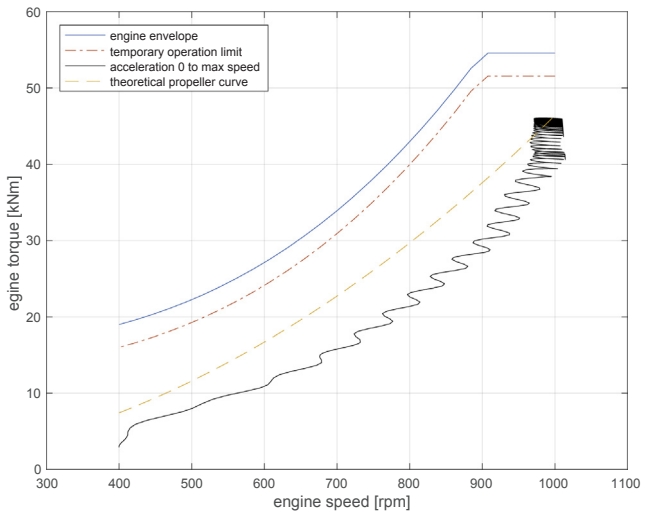

Fig. 31. Slam start acceleration from stationary to maximum speed in engine operating envelope for fast adaptive pitch control strategy with air excess ratio limitation $\lambda_{lim} = 1.45$ in trial and design conditions.

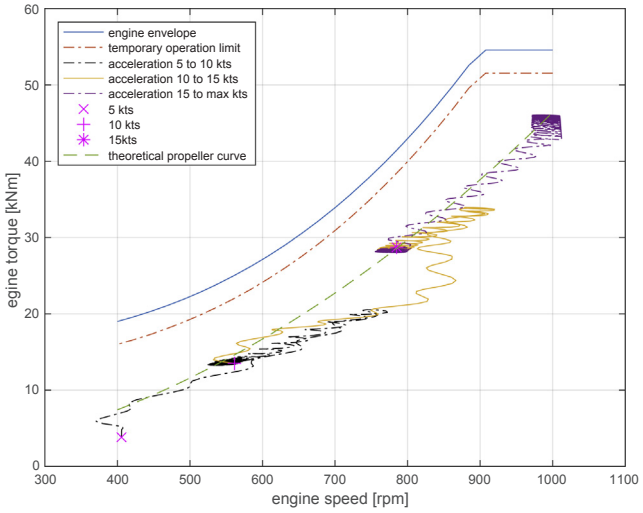

Fig. 32. Intermediate sprints in design conditions from 0 to 5 kts, 5 to 10 kts, 10 to 15 kts, and 15 kts to maximum ship speed in engine operating envelope for fast adaptive pitch control strategy with air excess ratio limitation $\lambda_{\text{lim}} = 1.45$ in trial and design conditions.

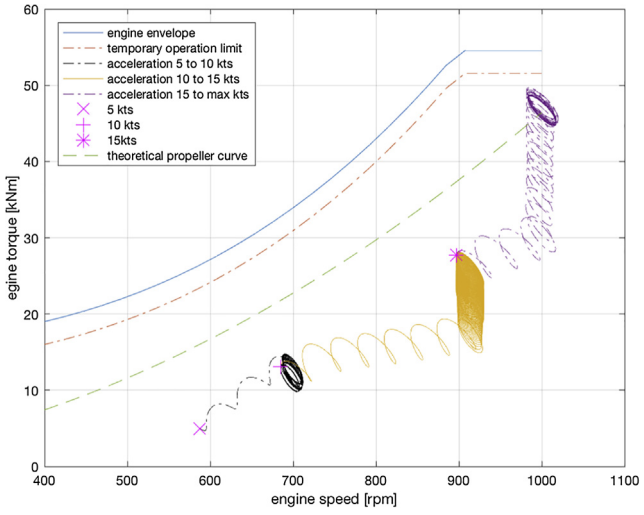

Fig. 34. Intermediate sprints in design conditions from 0 to 5 kts, 5 to 10 kts, 10 to 15 kts, and 15 kts to maximum ship speed in engine operating envelope for baseline manoeuvre control strategy in trial and design conditions.

shown in Figs. 26 and 29. Acceleration is 32% faster with fast adaptive pitch control than with the baseline manoeuvre, as shown in Fig. 30, but a further increase in engine speed during the acceleration might enable even faster acceleration.

If the propulsion engines would be supported by an electric machine in a hybrid propulsion configuration, as proposed in [92,93], engine speed potentially could be increased even more, further reducing the effect of the turbocharger lag and reducing acceleration time. [92] shows that a combination of speed control on the induction machine and torque control of the main engine would reduce acceleration time by 40% compared to acceleration time without the electric machine, when a fixed combinator curve is used. Future work should investigate how much acceleration time can be further reduced with the combination of the proposed adaptive pitch control strategy and parallel control of an electric drive and propulsion diesel engine.

4.3.6. Prevent engine overspeed and under-speed

The control objective to prevent engine over- and under-speed is achieved by hard over- and under-speed limitations defined in (36) and (37) and by switching from slow integrating speed control (34) to fast *PI* speed control (45). Fig. 35 shows that fuel injection is limited during speed fluctuations in design conditions at the maximum virtual shaft speed setting, limiting engine overspeed to below 1050 rpm. Moreover, it shows how during the crash stop deceleration, [94,89], engine under-speed is prevented by switching to fast *PI* speed control (45), and how the fuel rack limitation that prevents engine under-speed is not even used during the crash stop manoeuvre. While slow integrating speed control does cause a 50 % increase in speed fluctuation due to heavy seas, from 30 rpm to 45 rpm, as illustrated in Figs. 16 and 17, engine speed stability is maintained in all conditions.

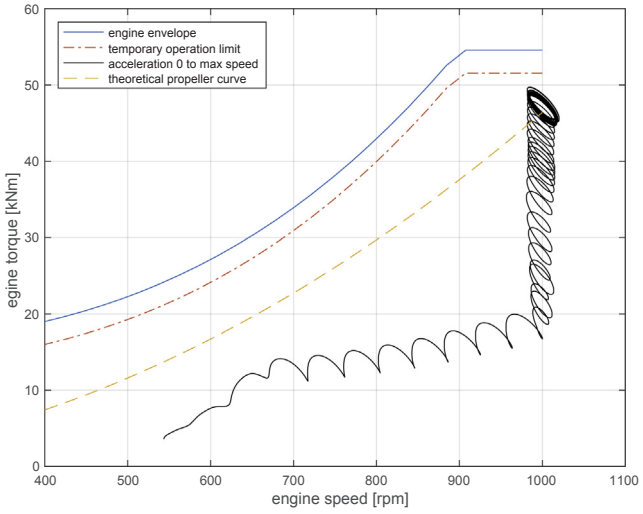

Fig. 33. Slam start acceleration from stationary to maximum speed in engine operating envelope for baseline manoeuvre control strategy in trial and design conditions.

4.4. Behaviour in waves and turns

The results in all operating envelopes above, Figs. 21, 22, 31, 32, 33 and 34, demonstrate that the adaptive pitch control strategy reduces the torque fluctuations due to waves, because slow integrating speed control attenuates torque fluctuations at the cost of a slight increase in engine speed fluctuations. Moreover, the adaptive pitch control strategy aims to maintain the angle of attack constant and tries to compensate

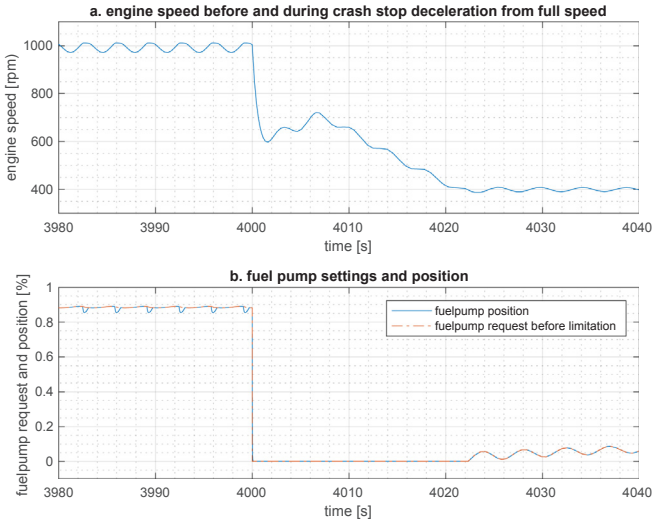

Fig. 35. Engine speed and fuel pump request and position during sailing at maximum speed and crash stop deceleration with fast adaptive pitch control in design conditions.

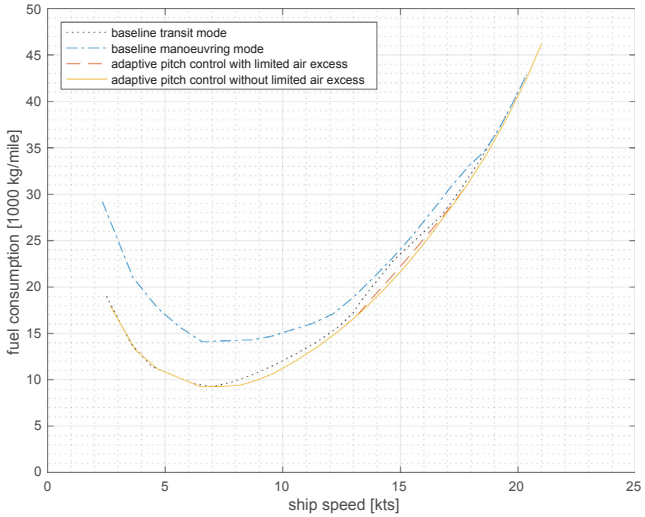

Fig. 36. Fuel consumption plot as a function of ships speed for trial conditions in manoeuvring and transit mode and with adaptive pitch control with and without limited air excess ratio.

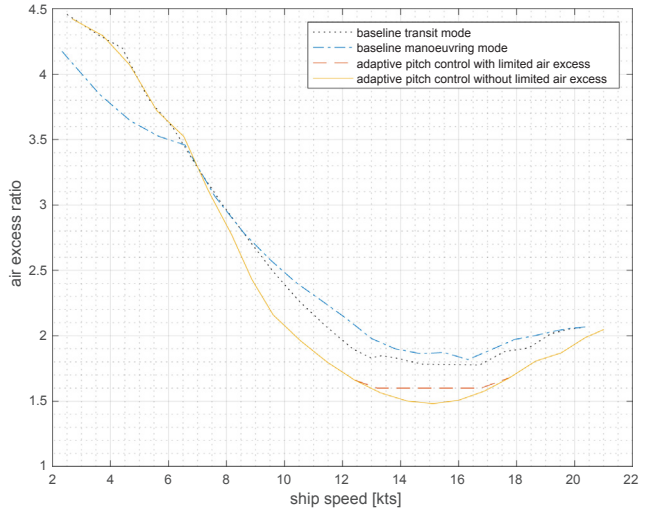

Fig. 38. Air excess ratio plot as a function of ships speed for trial conditions in manoeuvring and transit mode and with adaptive pitch control with and without limited air excess ratio.

the wake speed fluctuations from waves. However, due to the slow response of pitch actuation, the angle of attack during waves is not kept constant. While faster pitch actuation might enable the adaptive pitch control strategy to better maintain a constant angle of attack during high frequency wake fluctuations, we expect that the adaptive pitch control strategy can compensate for the relative slow wake speed fluctuations due to turns, particularly in stabilised conditions, as reported in [23, Fig. 3]. Moreover, the method to establish the angle of attack as described in [33] also uses the assumption of constant propeller characteristics, which [23] suggests also to hold for estimating the effect in turns, even though effects such as non-uniform wake distribution and oblique propeller inflow due to turns will have an impact on the accuracy of this assumption. Therefore, future work should be performed, first with simulation models and subsequently with model or full scale trials, to establish whether the adaptive pitch control strategy can also maintain the angle of attack in turns, thus reducing cavitation noise and increasing propeller and propulsion efficiency.

4.5. Measures of performance

The MOPs of the proposed adaptive pitch control strategy with and without a limited air excess ratio can now be compared with the MOPs of the transit and manoeuvre mode of the baseline control strategy as discussed in [24]. The fuel consumption plot for trial and design conditions, the air excess ratio plot for trial conditions, the cavitation plots for trial and design conditions and the angle of attack plot for trial conditions are shown in Figs. 36, 37, 38, 14, 15 and 39, for the three control strategies. Moreover, the acceleration time, minimum air excess ratio and maximum angle of attack of the transit and manoeuvre mode of the baseline control strategy and the proposed adaptive pitch control strategy with a limited air excess ratio are presented in Table 4.

From the comparison of the MOPs, we can draw the following conclusions:

- The adaptive pitch control strategy reduces fuel consumption in design conditions by 5–15% compared to the baseline transit mode in the ship speed range from 6 to 15 kts, and by 5–30% compared to the baseline manoeuvre mode in the speed range up to 15 kts. This is

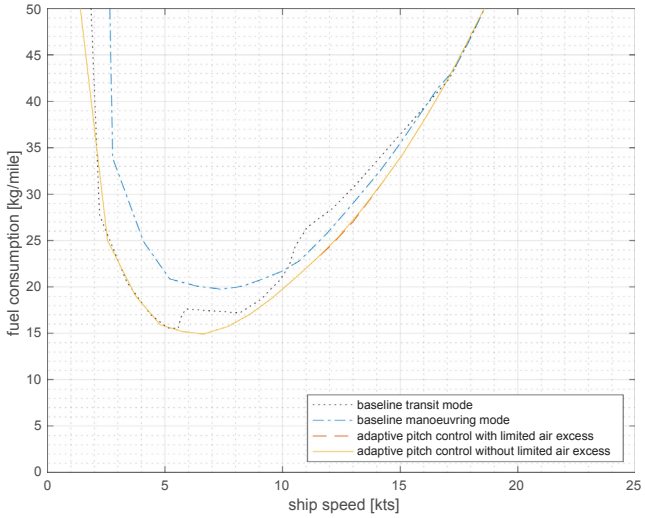

Fig. 37. Fuel consumption plot as a function of ships speed for design conditions in manoeuvring and transit mode and with adaptive pitch control with and without limited air excess ratio.

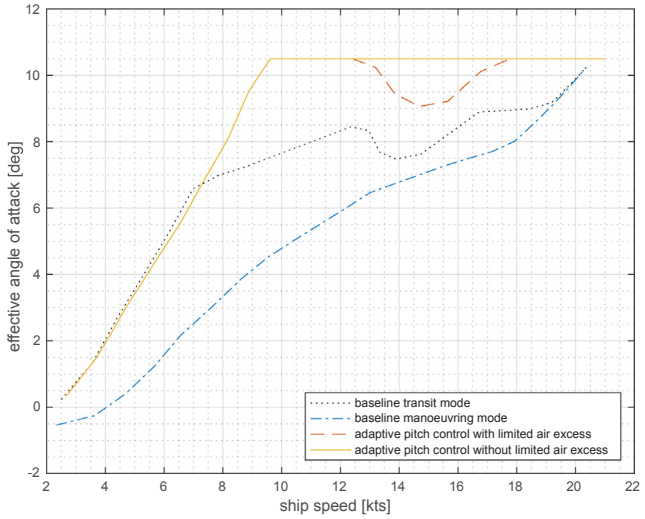

Fig. 39. Angle of attack plot from low speed to maximum speed for trial conditions in manoeuvring and transit mode and with adaptive pitch control with and without limited air excess ratio.

Table 4
Acceleration time, minimum air excess ratio and maximum angle of attack during acceleration with baseline control in manoeuvring (man) and transit (tran) mode compared with the proposed adaptive pitch control (apc) strategy (design condition).

Control strategy	tran	man	apc	Slow apc
Acceleration time (s): 0–5 kts	418	332	325	329
Acceleration time (s): 5–10 kts	253	154	87	98
Acceleration time (s): 10–15 kts	452	382	64	96
Acceleration time (s): 0–15 kts	203	111	89	139
Air excess ratio: 0–5 kts	2.43	2.50	1.93	2.07
Air excess ratio: 5–10 kts	1.68	1.66	1.45	1.51
Air excess ratio: 10–15 kts	1.69	1.62	1.45	1.45
Air excess ratio: 0–15 kts	1.75	1.70	1.47	1.51
Angle of attack (deg): 0–5 kts	13.6	10.0	12.5	12.7
Angle of attack (deg): 5–10 kts	10.9	9.0	12.3	12.5
Angle of attack (deg): 10–15 kts	10.8	9.1	11.4	11.7
Angle of attack (deg): 0–15 kts	10.3	11.1	12.5	12.7

achieved by running the engine at the theoretical propeller curve on the associated air excess ratio. When the air excess ratio is limited at 1.6, in the engine speed range from 600 to 800 rpm the engine torque is actually limited at a value below the theoretical propeller curve, causing a slight increase in fuel consumption of up to 2%, because the air excess ratio at 700 rpm on the propeller curve is 1.5, as shown in Fig. 9. Nevertheless, this would be a very conservative setting as the theoretical propeller curve lies well within the operating envelope of the engine.

- The adaptive pitch control strategy reduces acceleration time from 0 to 15 kts with the slam start procedure by 32% compared to the baseline manoeuvre mode and by 63% compared to the transit mode, while consistently maintaining the air excess ratio at a minimum value of 1.6. For an intermediate acceleration from 10 to 15 kts, acceleration time reduces by 84%. While faster acceleration can be achieved by using the slam start procedure [89], requesting maximum virtual start speed in stead of the virtual shaft speed associated with 15 kts, the adaptive pitch control strategy does provide a more consistent acceleration time, also for intermediate acceleration, without thermally overloading the engine.
- During acceleration, the angle of attack is kept around the design value of 10.5 deg, as shown in Figs. 14–17. The wake flow fluctuation causes the angle of attack to fluctuate with a similar amplitude as with the baseline control strategy.

In summary, the adaptive pitch control strategy accelerates much faster and much more consistently than the baseline manoeuvre mode, while also reducing fuel consumption significantly, without thermally overloading the engine and reducing cavitation risk for a propeller designed for low cavitation. Moreover, the control strategy does not need operator input to switch between fuel efficient or manoeuvrable operation.

5. Conclusions and future research

While shipping urgently needs to reduce its impact on the environment due to emissions and noise, multifunction ships also need to manoeuvre fast and accurate with a reliable propulsion plant to support more autonomous operation. This study has proposed an adaptive pitch control strategy for diesel mechanical or hybrid propulsion with slow integrating speed control and demonstrated the following: it robustly follows the requested virtual shaft speed; operates the propeller around its effective angle of attack; reduces fuel consumption and has the potential to improve NO_x and particulate matter (PM) emissions; maintains the air excess ratio λ at its required minimum value, thus limiting engine thermal loading; reduces acceleration time particularly during intermediates sprints, due to its consistent acceleration behaviour; and robustly prevents engine over- and under-speed. For the case study patrol vessel, the adaptive pitch control strategy reduces fuel consumption by 5–15% compared to the baseline transit mode in the ship speed range from 6 to 15 kts, and reduces acceleration time from 0 to 15 kts with the slam start procedure by 32% compared to the baseline manoeuvre mode and by 84% for an intermediate acceleration from 10 to 15 kts, without thermally overloading the engine.

Future work should establish how much NO_x and particulate matter (PM) emissions can be reduced with this strategy, as an initial analysis in this study suggests the proposed approach can be used to address the quasi-static trade-off between fuel consumption and NO_x emissions based on static maps, and the smooth torque trajectory due to slow integrating speed control is expected to have a positive impact on PM emissions. Moreover, the exact relation between charge pressure and engine thermal loading, indicated by exhaust valve and exhaust receiver temperatures should be established with simulation studies verified by experiments, to improve the fuel injection limitation that prevents engine thermal overloading. Finally, the maximum acceleration improvement and fuel consumption reduction with hybrid propulsion should be established, with an electric drive assisting the engine during acceleration and allowing more freedom of control in operating the main engine at its best possible fuel consumption.

With the proposed adaptive control strategy and these additional improvements, the freedom of control provided by controllable pitch propeller can be optimally utilised to contribute to the urgently required reduction of the environmental impact of shipping, both due to emissions and noise, without operator input. Moreover, the improvements in acceleration performance and reduction in engine thermal loading ensure the ships can be used for its increasingly divers tasks without operator input and with minimum time in port for maintenance, thus supporting more autonomous operation.

Acknowledgement

This project is partially supported by project ‘ShipDrive: A Novel Methodology for Integrated Modelling, Control, and Optimization of Hybrid Ship Systems’ (project 13276) of the Netherlands Organisation for Scientific Research (NWO), domain Applied and Engineering Sciences (TTW) and by the Royal Netherlands Navy. The Royal Netherlands Navy supplied Fig. 2. Special thanks goes to dr. Arthur Vrijdag for providing advice to improve the scientific quality and readability of this article.

Appendix A. Supplementary data

Supplementary data associated with this article can be found, in the online version, at https://doi.org/10.1016/j.apenergy.2018.07.080.

References

[1] UN. The emissions gap report 2017, Tech. rep. United Nations Environment Programme, November 2017.
[2] IMO MEPC 72. Initial strategy on greenhouse gas emissions from ship, Tech. rep. International Maritime Organisation (IMO), April 2018.
[3] Li S, Negenborn RR, Lodewijks G. Closed-loop coordination of inland vessels operations in large seaports using hybrid logic-based benders decomposition. Transport Res Part E: Logist Transport Rev 2017;97:1–21. https://doi.org/10.1016/j.tre.2016.10.013.
[4] Li S, Negenborn RR, Lodewijks G. Planning inland vessel operations in large seaports using a two-phase approach. Comp Indust Eng 2017;106:41–57. https://doi.org/10.1016/j.cie.2017.01.027.
[5] Zheng H, Negenborn RR, Lodewijks G. Closed-loop scheduling of waterborne AGVs for energy-efficient inter terminal transport. Transport Res Part E: Logist Transport Rev 2017;105:261–78. https://doi.org/10.1016/j.tre.2016.07.010.
[6] Zheng H, Negenborn RR, Lodewijks G. Fast ADMM for distributed model predictive control of cooperative waterborne agvs. IEEE Trans Control Syst Technol 2017;25(4):1406–13. https://doi.org/10.1109/TCST.2016.2599485.
[7] Chen L, Yip TL, Mou J. Provision of emission control area and the impact on shipping route choice and ship emissions. Transport Res Part D: Transport Environ 2017, doi:https://doi.org/10.1016/jtrd.2017.07.003 [in press].

[8] Vettor R, Guedes Soares C. Development of a ship weather routing system. Ocean Eng 2016;123:1014. https://doi.org/10.1016/j.oceaneng.2016.06.035.

[9] Perera LP, Soares CG. Weather routing and safe ship handling in the future of shipping. Ocean Eng 2017;130:684–95. https://doi.org/10.1016/j.oceaneng.2016.09.007.

[10] Coraddu A, Figari M, Savio S. Numerical investigation on ship energy efficiency by monte carlo simulation. Proc IMechE Part M: J Eng Marit Environ 2014;228(3):220–34. https://doi.org/10.1177/1475090214524184.

[11] Roskilly AP, Palacin R, Yan J. Novel technologies and strategies for clean transport systems. Appl Energy 2015;157:563–6. https://doi.org/10.1016/j.apenergy.2015.09.051.

[12] Taljegard M, Brynolf S, Grahn M, Andersson K, Johnson H. Cost-effective choices of marine fuels in a carbon-constrained world: results from a global energy model. Environ Sci Technol 2014;48:12986–93. https://doi.org/10.1021/es5018575.

[13] Brynolf S, Baldi F, Johnson H. Shipping and the environment. Berlin (Heidelberg): Springer; 2016. p. 295–339, doi:https://doi.org/10.1007/978-3-662-49045-7 [Ch. Energy Efficiency and Fuel Changes to Reduce Environmental Impacts].

[14] Shu G, Liang Y, Wei H, Zhao J, Liu l. A review of waste heat recovery on two-stroke ic engine aboard ships. Renew Sustain Energy Rev 2013;19:385–401. https://doi.org/10.1016/j.rser.2012.11.034.

[15] Cignitti S, Andreasen JG, Haglind F, Woodley JM, Abildskov J. Integrated working fluid-thermodynamic cycle design of organic rankine cycle power system for waste heat recovery. Appl Energy 2017;203:442–53. https://doi.org/10.1016/j.apenergy.2017.06.031.

[16] Mondejar ME, Ahlgren F, Thern M, Genrup M. Quasi-steady state simulation of an organic rankine cycle for waste heat recovery in a passenger vessel. Appl Energy 2017;185(2):1324–35. https://doi.org/10.1016/j.apenergy.2016.03.024.

[17] Benvenuto G, Campora U, Trucco A. Comparison of ship planting layouts for power and propulsion systems with energy recovery. J Mar Eng Technol 2014;13(3):3–15. https://doi.org/10.1080/20464177.2014.11658117.

[18] De La Fuente SS, Greig AR. Making shipping greener: comparative study between organic fluids and water for rankine cycle waste heat recovery. J Mar Eng Technol 2015;14:2:70–84. https://doi.org/10.1080/20464177.2015.1077601.

[19] Georgescu I, Godjevac M, Visser K. Efficiency constraints of energy storage for on-board power systems. Ocean Eng 2018;162:239–47. https://doi.org/10.1016/j.oceaneng.2018.05.004.

[20] Zahedi B, Norum LE, Ludwigsen KB. Optimised efficiency of all-electric ship by dc hybrid power systems. J Power Sour 2014;255:341–54.

[21] Geertsma RD, Negenborn RR, Visser K, Hopman JJ. Design and control of hybrid power and propulsion systems for smart ships: a review of developments. Appl Energy 2017;194:30–54. https://doi.org/10.1016/j.apenergy.2017.02.060.

[22] Schulten PJM, Geertsma RD, Visser K. Energy as a weapon, part 2. In: Proceedings of the engine as a weapon VII conference. Bristol (UK); 2017.

[23] Coraddu A, Dubbioso G, Mauro S, Viviani M. Analysis of twin screw ships asympetric propeller behaviour by means of free running model tests. Ocean Eng 2013;68:47–64. https://doi.org/10.1016/j.oceaneng.2013.04.013.

[24] Geertsma RD, Negenborn RR, Visser K, Hopman JJ. Pitch control for ships with mechanical and hybrid propulsion: modelling, validation and performance quantification. Appl Energy 2017;206:1609–31. https://doi.org/10.1016/j.apenergy.2017.09.103.

[25] Klein Woud H, Stapersma D. Design of propulsion and electric power generation systems. London (UK): IMarEST; 2012.

[26] Martelli M, Figari M. Real-time model-based design for CODLAG propulsion control strategies. Ocean Eng 2017;14:265–76. https://doi.org/10.1016/j.oceaneng.2017.06.029.

[27] Martelli M. Marine propulsion simulation. Warsaw/Berlin: De Gruyter Open Ltd; 2014.

[28] Stapersma D. Matching propulsion engine with propulsor. J Mar Eng Technol 2005;4(2):25–32.

[29] Coraddu A, Gaggero S, Villa D, Figari M. A new approach in engine-propeller matching. In: Proceedings of the 14th international congress of the international maritime association of the mediterranean, IMAM 2011, vol. 2. p. 631–7.

[30] Vrijdag A, Stapersma D, van Terwisga T. Trade-offs in ship propulsion control: engine overloading and cavitation inception in operational conditions. In: Proceedings of the 9th international naval engineering conference. Hamburg (Germany); 2008. p. 82–93.

[31] Vrijdag A, Stapersma D, van Terwisga T. Control of propeller cavitation in operational conditions. J Mar Eng Technol 2010;16:15–26. https://doi.org/10.1080/20464177.2010.11020228.

[32] Vrijdag A, Schulten PJM, Stapersma D, van Terwisga T. Efficient uncertainty analysis of a complex multidisciplinary simulation model. J Mar Eng Technol 2007:10.

[33] Vrijdag A. Control of propeller cavitation in operational conditions, PhD thesis. TU Delft (The Netherlands): Faculty Mechanical, Maritime and Materials Engineering; 2009.

[34] Vrijdag A, Stapersma D, van Terwisga T. Systematic modelling, verification, calibration and validation of a ship propulsion simulation model. Proc IMarEST Part A: J Mar Eng Technol 2009;8(15):3–20.

[35] Faber E. Some thoughts in diesel marine engineering. SNAME Trans 1993;101:537–82.

[36] Stapersma D, Schulten PJM, Grimmelius HT. A fresh view on propulsion control. In: Proceedings of the 7th international naval engineering conference. Amsterdam (The Netherlands); 2004. p. 221–40.

[37] Stapersma D, Vrijdag A, Grimmelius HT. A fresh view on propulsion control II. In: Proceedings of the 14th international ship control systems symposium. Ottawa (Canada); 2009.

[38] Van Spronsen P, Toussain R. An optimal control approach to preventing marine diesel engine overloading aboard *Karel Doorman* class frigates. IFAC Proc Vol 2001;34(7):23–30. https://doi.org/10.1016/S1474-6670(17)35130-3.

[39] Guillemette JR, Bussières P. Proposed optimal controller for the Canadian patrol frigate diesel propulsion system. In: Proceedings of the 11th ship control systems symposium. Southampton (UK); 1997. p. 507–30.

[40] Xiros N. Robust control of diesel ship propulsion. London (UK): Springer-Verlag; 2002.

[41] Mizuno N, Miyazaki Y, Kudo Y. Marine engine control with multivariable adaptive extremum control scheme. IFAC Proc Vol 2010:155–60. https://doi.org/10.3182/20100915-3-DE-3008.00042.

[42] Stefanopoulou A, Smith R. Maneuverability and smoke emission constraints in marine diesel propulsion. Control Eng Pract 2000;8:1023–31.

[43] Nielsen KV, Blanke M, Eriksson L. Control-oriented model of molar scavenge oxygen fraction for exhaust recirculation in large diesel engines. Trans ASME, J Dynam Syst, Measur Control 2017;139:0210071–9.

[44] Sorensen AJ, Smogeli ON. Torque and power control of electrically driven marine propellers. Control Eng Pract 2009;17:1053–64. https://doi.org/10.1016/j.conengprac.2009.04.006.

[45] Smogeli ON, Sorensen AJ, Minsaas KJ. The concept of anti-spin thruster control. Control Eng Pract 2008;16:465–81. https://doi.org/10.1016/j.conengprac.2006.06.004.

[46] Bakkeheim J, Johansen TA, Smogelli ON, Sorensen AJ. Lyapunov-based integrator resetting with application to marine thruster control. IEEE Trans Control Syst Technol 2008;16(5):908–17. https://doi.org/10.1109/TCST.2007.916340.

[47] Sorensen AJ. Structural issues in the design and operation of marine control systems. Ann Rev Control 2005;29:125–49. https://doi.org/10.1016/j.arcontrol.2004.12.001.

[48] Blanke M, Pivano L, Johansen TA. An efficiency optimizing propeller speed control for ships in moderate seas - model experiments and simulation. IFAC Proc Vol 2007;7(1):329–36.

[49] Blanke M, Nielsen PB. The marine engine governor. In: Proceedings of the 2nd maritime communications and control conference; 1990. p. 11–9.

[50] Geertsma RD, Negenborn RR, Visser K, Hopman JJ. Torque control for diesel mechanical and hybrid propulsion for naval vessels. In: Proceedings of the 13th international naval engineering conference. Bristol (UK); 2016. p. 476–92.

[51] Kretschmann L, Burmeister H, Jahn C. Analyzing the economic benefit of unmanned autonomous ships: an exploratory cost-comparison between an autonomous and a conventional bulk carrier. Res Transport Bus Manage 2017;25:76–86. https://doi.org/10.1016/j.rtbm.2017.06.002.

[52] Colonna P, van Putten H. Dynamic modelling of steam power cycles. Part I - modelling paradigm and validation. Appl Therm Eng 2007;27(2):467–80. https://doi.org/10.1016/j.applthermaleng.2006.06.011.

[53] Schulten PJM, Stapersma D. Mean value modelling of the gas exchange of a 4-stroke diesel engine for use in powertrain applications. In: SAE Technical Papers; 2003, doi:https://doi.org/10.4271/2003-01-0219.

[54] Theotokatos G. On the cycle mean value modelling of a large two-stroke marine diesel engine. Proc IMechE, Part M: J Eng Marit Environ 2010;224(3):193–205. https://doi.org/10.1243/14750902JEME188.

[55] Guan C, Theotokatos G, Zhou P, Chen H. Computational investigation of large containership propulsion engine operation at slow steaming conditions. Appl Energy 2014;130:370–83. https://doi.org/10.1016/j.apenergy.2014.05.063.

[56] Sapra H, Godjevac M, Visser K, Stapersma D, Dijkstra C. Experimental and simulation-based investigations of marine diesel engine performance against static backpressure. Appl Energy 2017;204:78–92. https://doi.org/10.1016/j.apenergy.2017.06.111.

[57] Baldi F, Theotokatos G, Andersson K. Development of a combined mean value-zero dimensional model and application for a large marine four-stroke diesel engine simulation. Appl Energy 2015;154:402–15. https://doi.org/10.1016/j.apenergy.2015.05.024.

[58] Benvenuto G, Campora U. Dynamic simulation of a high-performance sequentially turbocharged marine diesel engine. Int J Engine Res 2002;3(3):115–25.

[59] Scappin F, Stefansson SH, Haglind F, Andreasen A, Larsen U. Validation of a zero-dimensional model for prediction of nox and engine performance for electronically controlled marine two-stroke diesel engines. Appl Therm Eng 2012;37:252–344. https://doi.org/10.1016/j.applthermaleng.2011.11.047.

[60] Raptosasios S, Sakellaridis NF, Papagiannakis RG, Hountalas DT. Application of a multi-zone combustion model to investigate the nox reduction potential of two-stroke marine diesel engines using EGR. Appl Energy 2015;157:814–23. https://doi.org/10.1016/j.apenergy.2014.12.041.

[61] Pang KM, Karvounis N, Walther JH, Schramm J. Numerical investigation of soot formation and oxidation processes under large two-stroke marine diesel engine-like conditions using integrated CFD-chemical kinetics. Appl Energy 2016;169:874–87. https://doi.org/10.1016/j.apenergy.2016.02.081.

[62] Godjevac M, Drijver J, de Vries L, Stapersma D. Evaluation of losses in maritime gearboxes. Proc IMechE, Part M: J Eng Marit Environ 2016;230(4):623–38. https://doi.org/10.1177/1475090215613814.

[63] Dang J, van den Boom H, Ligtelijn JT. The Wageningen C- and D-series propellers. In: Proceedings of the 12th FAST conference. Amsterdam (The Netherlands); 2013.

[64] Dang J, Brouwer J, Bosman R, Pouw C. Quasi-steady two-quadrant open water tests for the Wageningen Propeller C- and D-series. In: Proceedings of the 29th symposium on naval hydrodynamics. Gothenburg (Sweden); 2012.

[65] Grimmelius HT, Bakker JC, Wesselink AF. The use of non linear models in the analysis of cpp actuator behaviour. In: Marine engineering systems. London (UK): IMarEST; 2006. p. 240–54.

[66] Wesselink AF, Stapersma D, van den Bosch D. Non-linear aspects of propeller pitch control. In: Proceedings of the 8th international naval engineering conference.

London (UK); 2006.
[67] Godjevac. Wear and friction in a controllable pitch propeller, PhD thesis. Faculty Mechanical, Maritime and Materials Engineering, Delft University of Technology; 2009.
[68] Schulten PJM. The interaction between diesel engines, ship and propellers during manoeuvring, PhD thesis. Faculty Mechanical, Maritime and Materials Engineering, Delft University of Technology; 2005.
[69] Taskar B, Yum KK, Steen S, Pedersen E. The effect of waves on engine-propeller dynamics and propulsion performance of ships. Ocean Eng 2016;122:262–77. https://doi.org/10.1016/j.oceaneng.2016.06.034.
[70] Amini H, Steen S. Theoretical and experimental investigation of propeller shaft loads in transient conditions. Int Shipbuild Prog 2012;59:55–82. https://doi.org/10.3233/ISP-2012-0079.
[71] Gerritsma J, Beukelman W. Analysis of the resistance increase in waves of a fast cargo ship. Int Shipbuild Prog 1972;19(217):285–93.
[72] Gerritsma J. Bewegingen en sturen 1 - Golven, MT513, report 473-K. Faculty Mechanical, Maritime and Materials Engineering, Delft University of Technology; 1989.
[73] van Straaten OFA, de Boer MJ. Optimum propulsion engine configuration from fuel economic point of view. In: Proceedings of the 11th international naval engineering conference. Edinburgh (UK); 2012.
[74] Roedler GJ, Jones C. Technical measurement, a coll. project of PSM, INCOSE and industry, Technical Report INCOSE-TP-2003-020-01 v1.0. INCOSE; 2005.
[75] Sciarretta A, Serrao L, Dewangan PC, Tona P, Bergshoeff END, Bordons C, et al. A control benchmark on the energy management of a plug-in hybrid electric vehicle. Control Eng Pract 2014;29:287–98. https://doi.org/10.1016/j.conengprac.2013.11.020.
[76] Shi W. Dynamics of energy system behaviour and emissions of trailing suction hopper dredgers, PhD thesis. The Netherlands: Faculty Mechanical, Maritime and Materials Engineering, Delft University of Technology; 2013.
[77] Shi W, Grimmelius HT, Stapersma D. Analysis of ship propulsion system behaviour and the impact on fuel consumption. Int Shipbuild Prog 2010;57:35–64.
[78] MAN Diesel SE. Project guide for marine plants diesel engine 28/33d prelim., Tech. rep. Augsburg (Germany): MAN Diesel SE, May 2008.
[79] Geertsma RD, Vollbrandt J, Negenborn RR, Visser K, Hopman JJ. A quantitative comparison of hybrid diesel-electric and gas-turbine-electric propulsion for future frigates. In: Proceedings of the 2017 IEEE electric ship technologies symposium; 2017. p. 451–8.
[80] Grimmelius HT, Stapersma D. Control optimisation and load prediction for marine diesel engines using a mean value first principle model. In: Proceedings of the MS& TES conference. Newcastle-upon-Tyne (UK); 2000. p. 212–9.
[81] Grimmelius HT, Stapersma D. The impact of propulsion plant control on diesel engine thermal loading. In: Proceedings of the 22nd CIMAC world congress. Hamburg (Germany); 2001.
[82] Rubis CJ, Harper TR. Governing ship propulsion gas turbine engines. SNAME Trans 1986;94:283–308.
[83] Astrom KJ, Hagglund T. The future of PID control. Control Eng Pract 2001;9(11):1163–75. https://doi.org/10.1016/S0967-0661(01)00062-4.
[84] Ren Y, Li L, Brindley J, Jiang L. Nonlinear PI control for variable pitch wind turbine. Control Eng Pract 2016;50:84–94. https://doi.org/10.1016/j.conengprac.2016.02.004.
[85] de Boer M, Hardy I. Final dynamic simulations ps, Tech. Rep. E40800/E1200.58. Damen Schelde Naval Shipbuilding; 2011.
[86] Xiros NI. PID marine engine speed regulation under full load conditions for sensitivity $h-\infty$ norm specifications against propeller disturbance. J Mar Eng Technol 2014;3(2):3–11. https://doi.org/10.1080/20464177.2004.11020179.
[87] Stapersma D, Vrijdag A. Linearisation of a ship propulsion system model. Ocean Eng 2017;142:441–57. https://doi.org/10.1016/j.oceaneng.2017.07.014.
[88] Vrijdag A, Stapersma D. Extension and application of a linearised ship propulsion system model. Ocean Eng 2017;143:50–65. https://doi.org/10.1016/j.oceaneng.2017.07.023.
[89] Altosole M, Martelli M. Propulsion control strategies for ship emergency manoeuvres. Ocean Eng 2017;137:99–109. https://doi.org/10.1016/j.oceaneng.2017.03.053.
[90] Haseltalab A, Negenborn R. Adaptive control for a class of partially unknown non-affine systems: applied to autonomous surface vessels. IFAC Proc Vol 2007;50-1:4252–7. https://doi.org/10.1016/j.ifacol.2017.08.830.
[91] Nuesch T, Wang M, Isenegger P, Onder CH, Steiner R, Macri-Lassus P, et al. Optimal energy management for a diesel hybrid electric vehicle considering transient pm and quasi-static nox emissions. Control Eng Pract 2014;29:266–76. https://doi.org/10.1016/j.conengprac.2014.01.020.
[92] Geertsma RD, Negenborn RR, Visser K, Hopman JJ. Parallel control for hybrid propulsion of multifunction ships. IFAC Proc Vol 2017;50(1):2296–303. https://doi.org/10.1016/j.ifacol.2017.08.229.
[93] Topaloglou S, Paplambrou G, Kyrtatos N. Energy management controller design for hybrid ship propulsion during transient operation. In: Proceedings of the 28th CIMAC, 50. Helsinki (Finland); 2016. p. 1–9.
[94] Altosole M, Marteli M, Vignolo S. A mathematical model of the propeller pitch change mechanism for the marine propulsion control design. In: Proceedings of the 14th congress of the international maritime association of the Mediteranean 2. Genova (Italy); 2012. p. 649–56.